

CHAPTER 4

Results and discussion

4.1. The percentage yields of medicinal plant extracts and essential oils

The dried leaves of *G. pictum*, *S. spirale* and *G. divaricata* were extracted using different methods and solvents.

The dried leaves of *G. pictum* (281.46 g) were macerated in hexane [**P1H**], CHCl₃ [**P1C**] and 95% EtOH [**P1E**] at room temperature for 3 days. The second batch (520.90 g) was macerated in hexane [**P1H2**], CH₂Cl₂ [**P1D**], and MeOH [**P1M**] at room temperature for 3 days. The last batch (583.36 g) was extracted with 95% EtOH [**PP1E**] for a week and then partitioned with hexane [**PP1H**], EtOAc [**PP1EA**] and *n*-BuOH [**PP1B**], respectively.

The dried stems of *S. spirale* (142.71 g) were macerated in hexane [**P2H**], CHCl₃ [**P2C**] and MeOH [**P2M**] at room temperature for a week.

The dried leaves of *G. divaricata* (472.0 g) were macerated in hexane [**P3H**], CH₂Cl₂ [**P3D**] and MeOH [**P3M**] at room temperature for 3 days and the second batch (142.75 g) was extracted using a Soxhlet extractor and petroleum spirit [**SP3P**], EtOAc [**SP3EA**] and 95% EtOH [**SP3E**], respectively.

Moreover, the fresh leaves of *G. pictum* and *G. divaricata* were selected to extract the essential oils. The fresh leaves of *G. pictum* (5.06 kg) and the fresh leaves of *G. divaricata* (1.83 kg) were homogenized and hydrodistilled in a modified Clevenger-type apparatus for 6 h to collect the essential oils [**OP1**] and [**OP3**], respectively. These essential oils were stored at 4 °C until further analysis.

The percentage yields of all crude extracts were calculated based on their dry weights, while the percentage yields of the essential oils were calculated based on their fresh weights. The results are shown in Table 4.1.

Table 4.1 The amount and percentage yields of the extracts, fractions and the essential oils from three medicinal plants: *G. pictum*, *S. spirale* and *G. divaricata*

Plants/methods	Extracts/fractions/essential oils ^a	Weight (g)	%yield
<i>G. pictum</i> leaves			
Maceration	[P1H]	2.06	0.73
	[P1C]	3.92	1.39
	[P1E]	8.42	2.99
Maceration	[P1H2]	4.20	0.81
	[P1D]	8.69	1.67
	[P1M]	12.64	2.43
Solvent partitioning	[PP1E]	66.29	11.36
	[PP1H]	24.31	4.17
	[PP1EA]	0.90	0.15
	[PP1B]	21.03	3.61
	[PP1A]	9.36	1.61
Distillation	[OP1]	0.0118	0.0002
<i>S. spirale</i> stems			
Maceration	[P2H]	1.07	0.75
	[P2C]	1.69	1.19
	[P2M]	10.08	7.06
<i>G. divaricata</i> leaves			
Maceration	[P3H]	9.83	2.08
	[P3D]	8.95	1.90
	[P3M]	8.81	1.87
Soxhlet extraction	[SP3P]	3.34	2.26
	[SP3EA]	3.70	2.50
	[SP3E]	8.72	5.89
Distillation	[OP3]	0.1424	0.0078

^a H = hexane, C = chloroform, E = ethanol, D = dichloromethane, M = methanol, EA = ethyl acetate, B = *n*-butanol, A = aqueous, P = petroleum spirit.

In the maceration method, the MeOH and EtOH extracts from *G. pictum* and *S. spirale* gave the highest percentage yields. The CHCl₃ and CH₂Cl₂ extracts gave moderate percentage yields and the hexane extracts gave the lowest percentage yields. On the other hand, *G. divaricata* leaves gave the hexane extract in the highest percentage yield (2.08%) followed by the CH₂Cl₂ (1.90%) and the MeOH (1.87%) extracts, respectively (Table 4.1).

The solvent partitioning of *G. pictum* leaves started with the maceration of the dried leaves with 95% EtOH at room temperature for a week, with shaking every day. After 7 days-maceration, the extract was filtered and dried using a rotary evaporator to receive the 95% EtOH extract 11.36 %w/w. This extract was further partitioned with hexane, EtOAc and *n*-BuOH, respectively. The residue of the partition was an aqueous fraction. The partition yields of all fractions (%w/w) were 4.17, 0.15, 3.61 and 1.61%, respectively (Table 4.1).

In the soxhlet extraction of *G. divaricata* leaves, the EtOH extract gave the highest percentage yield followed by the EtOAc and petroleum spirit extracts, respectively.

In addition, the fresh leaves of *G. pictum* were subjected to hydrodistillation using a modified Clevenger-type apparatus to yield 0.0002 %w/w of a pale yellow oil, whereas the fresh leaves of *G. divaricata* gave a yellow oil in 0.0078 %w/w.

4.2. Analysis of the essential oils

4.2.1. The leaf essential oil of *G. pictum* [OP1]

Fresh leaves of *G. pictum* were homogenized and hydrodistilled for 6 h to yield a pale yellow oil of 0.0002 % (w/w). GC-FID and GC-MS analysis of the oil identified fourteen compounds, collectively accounting for 95.0% of the gas chromatographical components. A GC chromatogram is presented in Figure 4.1. The major constituents were phytol (75.7%), *n*-nonacosane (6.5%) and hexahydrofarnesyl acetone (2.6%). The components were identified by comparison of their mass spectra from NIST and NISTREP libraries and by their retention indices (RI) relative to *n*-alkane indices on a Rxi-5MS capillary column

with comparisons with the literature data (93-97). The components, their retention indices and percentage composition, in order of their elution, are summarized in Table 4.2 with peak areas expressed as a percentage of the total chromatographable components of the essential oil assuming equal relative FID response for each component. Five components, collectively accounting for 4.8% of the total chromatographical oil, could not be identified due to their relatively low abundance and/or lack of reference spectra.

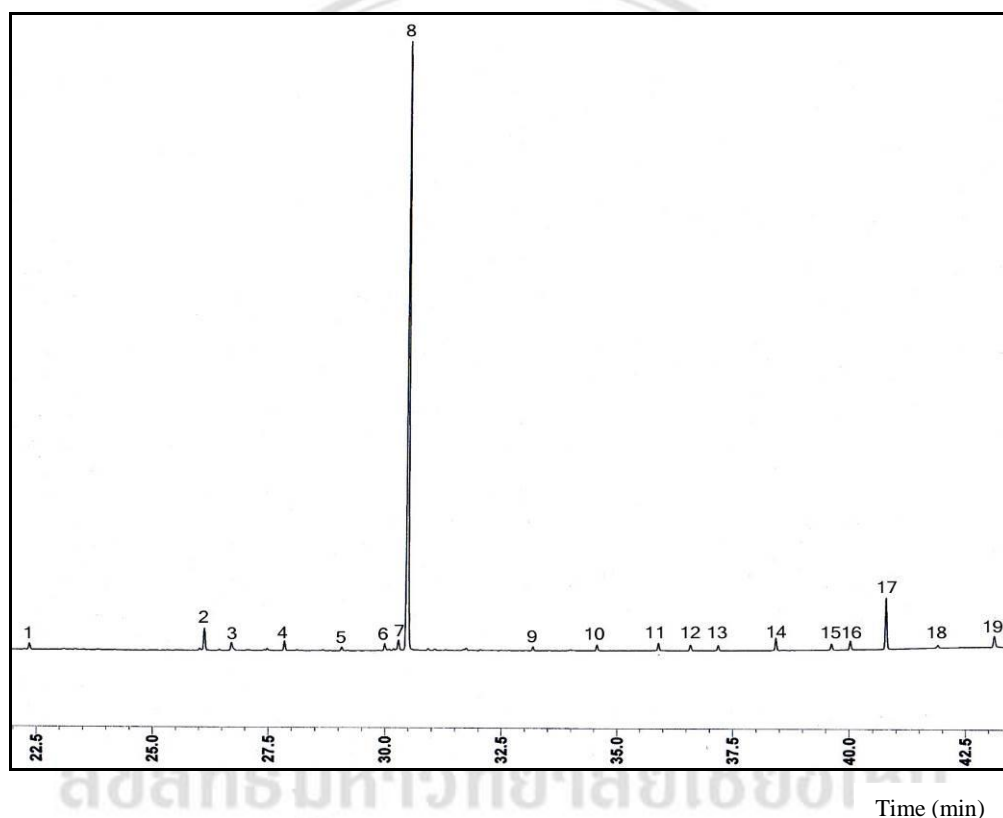


Figure 4.1 Gas chromatogram of the essential oil of *G. pictum* leaves

Table 4.2 Chemical constituents of the essential oil of *G. pictum*

Peak	Compounds	RA ^a (%)	RI(exp) ^b	RI(lit) ^c	Identification ^d	Ref
1	Unidentified ^e	0.8	1638	-	-	-
2	Hexahydrofarnesyl acetone	2.6	1847	1845	RI, MS	93
3	Unidentified	1.2	1881	-	-	-
4	Isophytol	1.1	1950	1946	RI, MS	94
5	Isopropyl palmitate	0.4	2026	2026.9	RI, MS	95
6	Unidentified	0.9	2084	-	-	-
7	Linolenic acid, methyl ester	1.4	2103	2098	RI, MS	96
8	Phytol	75.7	2116	2110	RI, MS	97
9	<i>n</i> -Tricosane	0.5	2300	2300	RI, MS	93,94
10	<i>n</i> -Tetracosane	0.7	2400	2400	RI, MS	93,94
11	<i>n</i> -Pentacosane	0.9	2500	2500	RI, MS	93,94
12	Unidentified	0.8	2554	-	-	-
13	<i>n</i> -Hexacosane	0.7	2600	2600	RI, MS	93,94
14	<i>n</i> -Heptacosane	1.6	2700	2700	RI, MS	93,94
15	<i>n</i> -Octacosane	0.8	2800	2800	RI, MS	93,94
16	Unidentified	1.1	2835	-	-	-
17	<i>n</i> -Nonacosane	6.5	2900	2900	RI, MS	93,94
18	<i>n</i> -Triacontane	0.4	3000	3000	RI, MS	93,94
19	<i>n</i> -Hentriacontane	1.7	3100	3100	RI, MS	93,94
Carbonylic compound		2.6				
Oxygenated acyclics diterpenes		76.8				
Fatty acid esters		1.8				
<i>n</i> -alkanes		13.8				
Unidentified (5 in total)		4.8				
Oil components (total)		99.8				

^aRA, relative area (peak area relative to total peak area); ^bRI(exp), programmed temperature retention indices as determined on a Rxi-5MS column using a homologous series of *n*-alkanes (C₇-C₃₀) as internal standard and H₂ as carrier gas; ^cRI(lit) values from literature data (93-97); ^dMS, From a comparison of the mass

spectrum with MS libraries and RI of literature; °EI MS m/z 204 (40%), 179 (31%), 161 (54%), 119 (100%).

The most abundant compounds in the oil were oxygenated acyclic diterpenes 76.8%, followed by *n*-alkanes 13.8%, a carbonylic compound 2.6%, and a small amount of fatty acid esters 1.8% (Table 4.2). The major component, phytol, is an oxygenated acyclic diterpene which can be produced from cleavage the phytol side chain of chlorophyll and has been subjected to catalytic cracking to produce gasoline in a renewable route to motor fuels (123). It can also be used as a precursor for the production of the synthetic forms of vitamin E (124) and vitamin K1 (125). In fragrance manufacturing, phytol and isophytol are used as ingredients in cosmetics, fine perfumes, shampoos, toilet soaps and other toiletries as well as in non-cosmetic products such as household cleaners and detergents (126-127).

4.2.2. The leaf essential oil of *G. divaricata* [OP3]

Fresh leaves of *G. divaricata* were homogenized and hydrodistilled to afford a yellow oil in 0.0078 % (w/w). The essential oil was analysed by GC-FID and GC-MS. A GC chromatogram is presented in Figure 4.2. Thirteen components were identified, representing 97.1% of the chromatographical fraction of the oil (Table 4.3). Oxygenated sesquiterpenes (73.3%) were the main group of the constituents followed by sesquiterpene hydrocarbons (11.9%), fatty acid (1.4%), oxygenated acyclic diterpene (1.3%), oxygenated monoterpene (0.9%) and monoterpene hydrocarbon (0.7%), respectively. Four components, collectively accounting for 7.6% of the total chromatographical oil, could not be identified due to their relatively low abundance and/or lack of reference spectra. The major compounds were cubenol (65.7%) and spathulenol (6.4%). These results were different from the previous studies on this plant. The first study showed that τ -cadinene (20.8%) and γ -elemene (10.6%) were the major components (77), while a more recent study, from plants collected in two different areas of China, revealed the major components of the essential oil were

α -pinene (49.7%) and β -caryophyllene (43.7%) in the first area and β -caryophyllene (48.2%) and limonene (21.0%) in the second area (78).

Cubenol was not identified as a component in this earlier study. This variation in the two major essential oil components might be because of the different plant locations (Thailand versus China), habitats and plant collection times. However, the minor components β -pinene, copaene, α -humulene, β -elemene, spathulenol, phytol and *n*-hexadecanoic acid were found in both this study and the earlier ones.

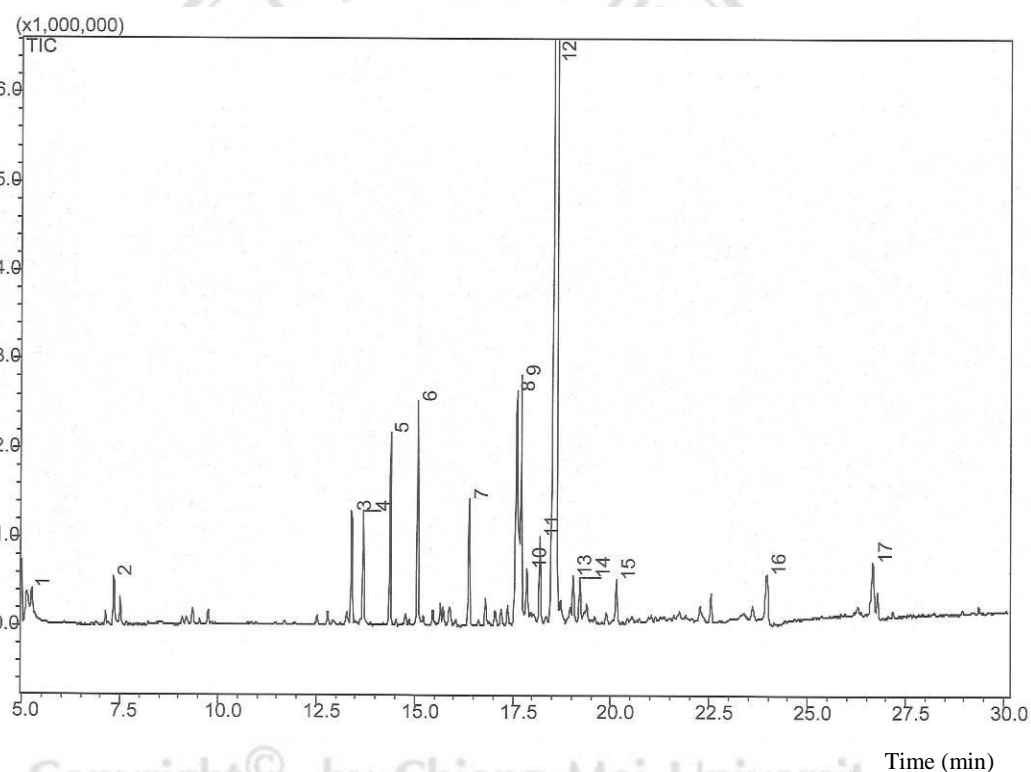


Figure 4.2 Gas chromatogram of the essential oil of *G. divaricata* leaves

Table 4.3 Chemical constituents of the essential oil from the fresh leaves of *G. divaricata*

Peak	Compounds	RA ^a (%)	RI(exp) ^b	RI(lit) ^c	Identification ^d	Ref
1	β -Pinene	0.7	982	981	RI, MS	98
2	Linalool	0.9	1100	1100	RI, MS	99
3	Copaene	1.7	1387	1391	RI, MS	100
4	β -Elemene	1.8	1400	1393	RI, MS	98
5	Aromadendrene	2.8	1434	1437	RI, MS	93
6	α -Humulene	3.0	1470	1467	RI, MS	99
7	δ -Cadinene	1.8	1535	1536	RI, MS	101
8	Spathulenol	6.4	1593	1591	RI, MS, ¹ H	102
9	Unidentified	4.2	1600	-	-	-
10	Viridiflorol	1.2	1609	1612	RI, MS	101
11	Unidentified	1.9	1627	-	-	-
12	Cubenol	65.7	1648	1645	RI, MS, ¹ H	99
13	Unidentified	0.8	1683	-	-	-
14	α -Calacorene ^e	0.8	1693	-	MS	-
15	Unidentified	0.7	1737	-	-	-
16	<i>n</i> -Hexadecanoic acid	1.4	1963	1957	RI, MS	93
17	Phytol	1.3	2156	2132	RI, MS	93
	Monoterpene hydrocarbon	0.7				
	Oxygenated monoterpene	0.9				
	Sesquiterpene hydrocarbons	11.9				
	Oxygenated sesquiterpenes	73.3				
	Fatty acid	1.4				
	Oxygenated acyclic diterpene	1.3				
	Unidentified (4 in total)	7.6				
	Oil components (total)	97.1				

^aRA, relative area (peak area relative to total peak area); ^bRI(exp), programmed temperature retention indices as determined on a Rxi-5MS column using a homologous series of *n*-alkanes (C₇-C₃₀) as internal standard and H₂ as carrier gas; ^cRI(lit) values from literature data; ^dMS, From a comparison of the mass spectrum

with MS libraries, RI of literature and $^1\text{H-NMR}$ (spathulenol (128), cubenol (129); $^{\circ}$ Tentative identification, RI(lit) have been reported as 1859 (99), 1744 (130) and 1540 (115).

4.3. Cytotoxic activity

The cytotoxicities of the essential oils of *G. pictum* [**OP1**] and *G. divaricata* [**OP3**], the crude extracts and the fractions of *G. pictum* ([**P1**] and [**PP1**]), and the crude extracts of *G. divaricata* ([**P3**] and [**SP3**]) were determined against the KB (epidermoid carcinoma of oral cavity), MCF-7 (breast adenocarcinoma) and NCI-H187 (small cell lung carcinoma) cancerous human-cell lines using the Resazurin microplate assay (REMA). Moreover, these crude extracts and fractions were also tested for their cytotoxicity against Vero cells (African green monkey kidney) using the Green Fluorescent Protein (GFP) detection method.

The essential oil of *G. pictum* [**OP1**] inhibited the growth of the KB and NCI-H187 cell lines and the Vero cell line with IC_{50} values of 27.04, 25.27 and 26.52 $\mu\text{g/mL}$, respectively. However, it did not inhibit the growth of the MCF-7 cell line (Table 4.4). Phytol was the major compound in this essential oil (Table 4.2); it should play an important role in the cytotoxicity of this essential oil. A previous study showed that phytol had cytotoxicity against KB (IC_{50} 11.95 $\mu\text{g/mL}$) and MCF-7 (IC_{50} 39.60 $\mu\text{g/mL}$) cell lines, but was non-cytotoxic to NCI-H187 and Vero cell lines (55). These contrasting results suggest that the other components of the essential oil, rather than phytol itself, are responsible for the cytotoxicity against NCI-H187 and Vero cells. While the inactivity of the oil against MCF-7 suggests that the other components of the oil inhibit or mask the cytotoxicity of phytol. Phytol has also been reported to have cytotoxicity against HT-29 human colon cancer cells, MG-63 osteosarcoma and AZ-521 gastric cancer cells (131) while hentriacontane, a minor component of [**OP1**] and the active component of Natto extracts, has been shown to have possible anti-tumor promoter activity (132).

Table 4.4 Cytotoxicity of the essential oil, the crude extracts and the fractions from *G. pictum* [P1] and *G. divaricata* [P3].

Sample	IC ₅₀ ^a (µg/mL)			
	KB	MCF-7	NCI-H187	Vero cells
<i>G. pictum</i> leaves				
[P1H]	inactive	inactive	inactive	inactive
[P1C]	inactive	inactive	inactive	inactive
[P1E]	inactive	inactive	inactive	inactive
[P1D]	inactive	inactive	inactive	inactive
[P1M]	inactive	inactive	inactive	inactive
[PP1E]	inactive	33.27	inactive	inactive
[PP1H]	inactive	38.66	inactive	inactive
[PP1EA]	inactive	26.01	inactive	inactive
[PP1B]	inactive	inactive	inactive	inactive
[PP1A]	inactive	20.41	inactive	inactive
[OP1]	27.04	inactive	25.27	26.52
<i>G. divaricata</i> leaves				
[P3H]	inactive	inactive	inactive	inactive
[P3D]	inactive	inactive	inactive	inactive
[P3M]	inactive	inactive	inactive	inactive
[SP3P]	inactive	inactive	inactive	inactive
[SP3EA]	inactive	inactive	inactive	inactive
[SP3E]	inactive	inactive	inactive	inactive
[OP3]	5.79	47.44	17.65	inactive
Ellipticine ^b	0.841	-	1.20	1.621
Doxorubicin ^b	0.610	9.16	0.095	-
Tamoxifen ^b	-	9.87	-	-

^aConcentration that killed 50% of cell lines; ^bAnticancer drugs used as positive controls.

The essential oil of *G. divaricata* [OP3] exhibited cytotoxicity against the KB, MCF-7 and NCI-H187 cell lines with the IC₅₀ values of 5.79, 47.44 and 17.65 µg/mL, respectively. It was non-cytotoxic against Vero cells (Table 4.4). From the constituents

of [OP3] (Table 4.3), the previous studies reported that spathulenol had weak cytotoxicity (IC₅₀ values > 20 µg/mL) against eight different human carcinogenic cell lines, including the KB cell line (133). While the minor components of this oil, β-elemene inhibited the growth of human non-small cell lung cancer H460 and A549 cells (IC₅₀ 40-60 µg/mL) (134) and α-humulene was active against several solid tumor cell lines, including MCF-7 (GI₅₀ 55-73 µM) (135). In addition, *n*-hexadecanoic acid (or palmitic acid) has shown cytotoxicity against human leukemic cells, MOLT-4, and also showed *in-vivo* antitumor activity in mice (136). The cytotoxic activity of [OP3] may be due to the activity or synergy effects of these compounds.

None of the crude extracts of *G. pictum* [P1] and *G. divaricata* ([P3] and [SP3]) showed activities against these cancer cell lines except the fractions of *G. pictum* [PP1]; the 95% EtOH [PP1E], hexane [PP1H], EtOAc [PP1EA] and aqueous [PP1A] fractions only inhibited the growth of MCF-7 cell lines with IC₅₀ values of 33.27, 38.66, 26.01 and 20.41 µg/mL, respectively (Table 4.4). From this result, the solvent partitioning method [P1] of *G. pictum* revealed cytotoxic activity against MCF-7, while the maceration method [PP1] proved inactive. This may be due to the solvent partitioning method giving fractions which are purer than the crude extracts from the maceration, so the small amount of active compound in each fraction can fully exhibit its cytotoxicity. Moreover, all crude extracts [P1] and the fractions of *G. pictum* [PP1], and all crude extracts of *G. divaricata* ([P3] and [SP3]) were non-cytotoxic against Vero cells. The results are shown in Table 4.4.

4.4. Antimycobacterial and anti-herpes simplex virus type-1 activities

Antimycobacterial activities of the essential oils of *G. pictum* [OP1] and *G. divaricata* [OP3] and the CH₂Cl₂ and the MeOH crude extracts of *G. pictum* ([P1D] and [P1M]) and *G. divaricata* ([P3D] and [P3M]) were determined against *Mycobacterium tuberculosis* H₃₇Ra using the Green Fluorescent Protein (GFP)-based fluorescent detection method. The results showed that all samples had no antimycobacterial activity except the essential oil of *G. divaricata* [OP3] which inhibited *M. tuberculosis* H₃₇Ra with a MIC of 50 µg/mL (Table 4.5). According to the constituents of [OP3] (Table 4.3), phytol had been reported to possess antituberculosis activity with a MIC value of

100 µg/mL against *M. tuberculosis* H₃₇Rv *in vitro* (137) and another experiment also found that phytol gave a MIC value of 12.5 mg/mL against *M. tuberculosis* H₃₇Rv *in vitro* (138). Moreover, *n*-hexadecanoic acid showed antituberculosis against *M. tuberculosis* H₃₇Rv with a MIC value of 25 µg/mL using the Microplate Alamar Blue Assay (139). Therefore, the antimycobacterial activity of [OP3] may be due to the activity of these components or the synergistic effects of these compounds. In contrast, the essential oils of *G. pictum* [OP1] had phytol as a major compound (Table 4.2) but showed no activity against *M. tuberculosis* H₃₇Ra. This result may suggest that the other components of [OP1] inhibit or mask the antimycobacterial activity of phytol.

Anti-herpes simplex virus type-1 (HSV-1) activities of the essential oils of *G. pictum* [OP1], the crude extracts and the fractions of *G. pictum* ([P1] and [PP1]), and the crude extracts of *G. divaricata* ([P3] and [SP3]) were determined against HSV-1 (ATCC VR260) with Green Fluorescent Protein (GFP) detection. The results showed that all samples were inactive against HSV-1 (Table 4.5).

Table 4.5 Antimycobacterial and anti-herpes simplex virus type-1 activities of the essential oil, the crude extracts and the fractions from *G. pictum* [P1] and *G. divaricata* [P3].

Samples	<i>M. tuberculosis</i> H ₃₇ Ra	HSV-1
	MIC ^a (µg/mL)	IC ₅₀ ^b (µg/mL)
<i>G. pictum</i> leaves		
[P1H]	-	inactive
[P1C]	-	inactive
[P1E]	-	inactive
[P1D]	inactive	inactive
[P1M]	inactive	inactive
[PP1E]	-	inactive
[PP1H]	-	inactive
[PP1EA]	-	inactive
[PP1B]	-	inactive
[PP1A]	-	inactive

Table 4.5 (continued)

Samples	<i>M. tuberculosis</i> H ₃₇ Ra	HSV-1
	MIC ^a (µg/mL)	IC ₅₀ ^b (µg/mL)
[OP1]	inactive	inactive
<i>G. divaricata</i> leaves		
[P3H]	-	inactive
[P3D]	inactive	inactive
[P3M]	inactive	inactive
[SP3P]	-	inactive
[SP3EA]	-	inactive
[SP3E]	-	inactive
[OP3]	50.00	-
Rifampicin ^c	0.003-0.025	-
Streptomycin ^c	0.156-0.313	-
Isoniazid ^c	0.023-0.046	-
Ofloxacin ^c	0.391-0.781	-
Ethambutol ^c	0.234-0.469	-
Acyclovir ^d	-	6.954

^aMinimum inhibitory concentration; ^bConcentration that killed 50% of cell lines; ^cAntimycobacterial drugs used as positive controls; ^dAnti-herpes simplex virus drug used as positive control.

4.5. Antimicrobial activity

The antibacterial activities of the essential oils of *G. pictum* [OP1] and *G. divaricata* [OP3] and the fractions of *G. pictum* [PP1] were determined using the disc diffusion assay against three bacteria (*Staphylococcus aureus* (ATCC 25923), *Pseudomonas aeruginosa* (ATCC 27853) and *Escherichia coli* (ATCC 25922), using vancomycin, amikacin and norfloxacin as positive controls. The antibacterial activities as MIC values were determined as the lowest concentration of the sample which inhibits the growth of bacteria. The results are shown in Table 4.6.

All fractions of *G. pictum* [PP1], at every concentration tested, did not inhibit these three bacterial strains, whereas the essential oil of *G. pictum* [OP1] had antibacterial activities against both *S. aureus* and *E. coli*, with the most potent activity at 1.18 and 3.53 mg/mL, respectively. This oil was not active against *P. aeruginosa*. Notably, the essential oils rich in nonacosane and hexahydrofarnesyl acetone, which comprise 9.1% of the oil of this study (Table 4.2), have shown broad spectrum antimicrobial activities (140-141).

Moreover, the essential oil of *G. divaricata* [OP3] showed antibacterial activities against *S. aureus*, *P. aeruginosa* and *E. coli*, with the MIC values of 10.0, 50.0 and 5.0 mg/mL, respectively (Table 4.6). The antibacterial activity of [OP3] may be the consequence of the antibacterial activity of its constituents (Table 4.3). Spathulenol has been reported to possess modest antimicrobial activity (MIC 136 µg/mL) against *S. aureus* and *Proteus mirabilis* (128). *n*-Hexadecanoic acid and phytol have been reported to possess antibacterial activity against *S. aureus* (142-143). Cubenol, isolated from the essential oil of *P. uviferum*, was one of the most active antibacterials of the sesquiterpene components (144).

Table 4.6 MIC values of the essential oils from *G. pictum* [OP1] and *G. divaricata* [P3], and the fractions from *G. pictum* [PP1].

Concentration of sample (mg/mL)	Diameter of inhibition zone (mm) ^a		
	Bacteria		
	<i>S. aureus</i>	<i>P. aeruginosa</i>	<i>E. coli</i>
<i>G. pictum</i> leaves			
[PP1H]			
25.0, 12.5, 6.25, 3.125 and 1.5625	-	-	-
[PP1EA]			
18.0, 9.0, 4.5, 2.25 and 1.125	-	-	-
[PP1B]			
24.0, 12.0, 6.0, 3.0 and 1.5	-	-	-
[PP1A]			
18.4, 9.2, 4.6, 2.3 and 1.15	-	-	-

Table 4.6 (continued)

[OP1]			
9.40	-	-	7.0
7.05	-	-	-
Concentration of sample (mg/mL)	Diameter of inhibition zone (mm)^a		
	Bacteria		
[OP1]	<i>S. aureus</i>	<i>P. aeruginosa</i>	<i>E. coli</i>
4.70	7.0	-	-
3.525	6.0	-	5.5
2.35	-	-	-
1.7625	6.0	-	-
1.175	5.5	-	-
MIC ^b (mg/mL)	1.175	-	3.525
<i>G. divaricata</i> leaves			
[OP3]			
100.0	-	-	-
70.0	-	-	5.5
50.0	6.0	6.0	5.5
30.0	6.0	-	6.0
10.0	6.0	-	6.0
5.0	-	-	6.0
2.5	-	-	-
MIC ^b (mg/mL)	10.0	50.0	5.0
Vancomycin (30 µg/disc) ^c	16.0	-	-
Amikacin (30 µg/disc) ^c	-	17.0	17.0
Norfloxacin (5 µg/disc) ^c	12.5	22.0	11.0
Ethanol ^d	-	-	-

^aInhibition zones are the mean diameter of disc 5 mm; ^bMinimum inhibitory concentration that inhibited the growth of the bacteria; ^cStandard antibiotics used as positive controls; ^dnegative control.

The antimicrobial activities of the crude extracts of *G. pictum* [P1] and *G. divaricata* [P3] at concentrations of 20 mg/mL were also determined using the agar diffusion assay. The samples were tested against the three aforementioned bacterial strains and three fungi; *Aspergillus flavus*, *Candida albican* and *Trichophyton mentagrophyte* using gentamicin and ketoconazole as positive controls. The results are shown in Table 4.7.

It is indicated that the hexane [P1H], CHCl₃ [P1C], EtOH [P1E], CH₂Cl₂ [P1D], and MeOH [P1M] extracts of *G. pictum* showed antibacterial activities against *P. aeruginosa* with inhibition zones of 12.0, 13.0, 13.0, 13.0 and 12.0 mm, respectively. While all crude extracts of *G. pictum* did not inhibit *S. aureus* and *E. coli*. In addition, all crude extracts of *G. pictum* showed antifungal activity against *A. flavus*, except the hexane [P1H] extract, with inhibition zones of 11.0 (for [P1C]), 11.0 (for [P1E]), 11.0 (for [P1D]) and 10.0 (for [P1M]) mm. The CHCl₃ [P1C], the EtOH [P1E] and the MeOH [P1M] extracts inhibited *C. albican* with the same inhibition zones of 10.0 mm. Moreover, the hexane [P1H] and the CHCl₃ [P1C] extracts were also active against *T. mentagrophyte* with the same inhibition zones of 10.0 mm.

Table 4.7 Antimicrobial activity of the crude extracts from *G. pictum* [P1] and *G. divaricata* [P3].

Sample	Diameter of inhibition zone ^a (mm)					
	Bacteria			Fungi		
	<i>S. aureus</i>	<i>P. aeruginosa</i>	<i>E. coli</i>	<i>A. flavus</i>	<i>C. albican</i>	<i>T. mentagrophyte</i>
<i>G. pictum</i> leaves						
[P1H]	-	12.0	-	-	-	10.0
[P1C]	-	13.0	-	11.0	10.0	10.0
[P1E]	-	13.0	-	11.0	10.0	-
[P1D]	-	13.0	-	11.0	-	-
[P1M]	-	12.0	-	10.0	10.0	-

Table 4.7 (continued)

Sample	Diameter of inhibition zone ^a (mm)					
	Bacteria			Fungi		
	<i>S. aureus</i>	<i>P. aeruginosa</i>	<i>E. coli</i>	<i>A. flavus</i>	<i>C. albican</i>	<i>T. mentagrophyte</i>
<i>G. divaricata</i> leaves						
[P3H]	-	12.0	-	10.0	10.0	-
[P3D]	-	-	-	10.0	12.0	13.0
[P3M]	11.0	15.0	-	10.0	13.0	14.0
Gentamicin ^b	35.0	27.0	27.0	-	-	-
Ketoconazole ^b	-	-	-	25.0	37.0	16.0
Ethanol ^c	-	-	-	-	-	-

^aInhibition zones are the mean cork borer (9 mm) diameter; ^bStandard antibiotics used as positive controls (gentamicin (75 µg/mL) and ketoconazole (250 µg/mL)); ^c negative control.

The antibacterial and fungal activities of the crude extracts of *G. divaricata* are shown in Table 4.7. The MeOH extract [P3M] exhibited antibacterial activity against *S. aureus* and *P. aeruginosa* with inhibition zones of 11.0 and 15.0 mm, respectively. The hexane extract [P3H] only showed antibacterial activity against *P. aeruginosa* with an inhibition zone of 12.0 mm, while the CH₂Cl₂ extract [P3D] had no antibacterial activity against all tested bacterial strains. The CH₂Cl₂ [P3D] and the MeOH [P3M] extracts exhibited antifungal activities against *A. flavus*, *C. albican* and *T. mentagrophyte* with inhibition zones of 10.0, 12.0 and 13.0 mm (for [P3D]) and 10.0, 13.0 and 14.0 mm (for [P3M]), respectively. The hexane extract [P3H] showed antifungal activity against *A. flavus* and *C. albican* with the same inhibition zones of 10.0 mm.

4.6. Antioxidant activity

4.6.1. ABTS method

The ABTS assay is a decolorization assay which starts with the generation of the greenish blue ABTS radical cation (ABTS^{•+}) by oxidation of ABTS (2,2'-azinobis-(3-ethylbenzothiazoline-6-sulfonic acid) with potassium

persulfate. The ABTS^{•+} is reduced by accepting an electron from the antioxidant. The discolorization of ABTS^{•+} was determined by the absorbance at 734 nm (145).

The antioxidant activities of the essential oil [OP1] and the fractions [PP1] of *G. pictum* and the essential oil of *G. divaricata* [OP3] were investigated using the ABTS radical cation scavenging assay by comparison with the standards, trolox and ascorbic acid. A series of standard solutions containing: 0.13-0.63 mg/mL of trolox and 0.09-0.44 mg/mL of ascorbic acid solutions were prepared. The percentage inhibition of each concentration of trolox is shown in Table 4.8, whereas the percentage inhibition of each concentration of ascorbic acid is shown in Table 4.9. The percentage inhibitions were plotted against the trolox and ascorbic acid concentrations to obtain the linear calibration curves which gave the linear regression equations for trolox and ascorbic acid (Figure 4.3-4.4; for the essential oils and Figure 4.5-4.6; for the fractions). This standard linear regression equation was used to calculate the equivalent capacity of each sample.

Table 4.8 The percentage inhibition of trolox solution by ABTS method

Concentration of trolox (mg/mL)	% inhibition	
	essential oils	fractions
0.13	19.75	17.53
0.25	36.79	37.54
0.38	57.68	57.50
0.50	76.35	73.51
0.63	92.54	90.47

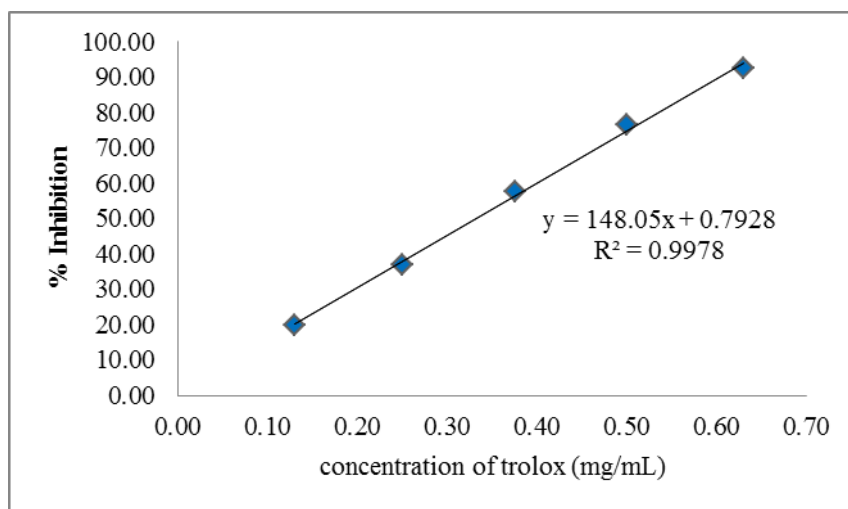


Figure 4.3 Calibration curves of standard trolox solution by ABTS method for the essential oils

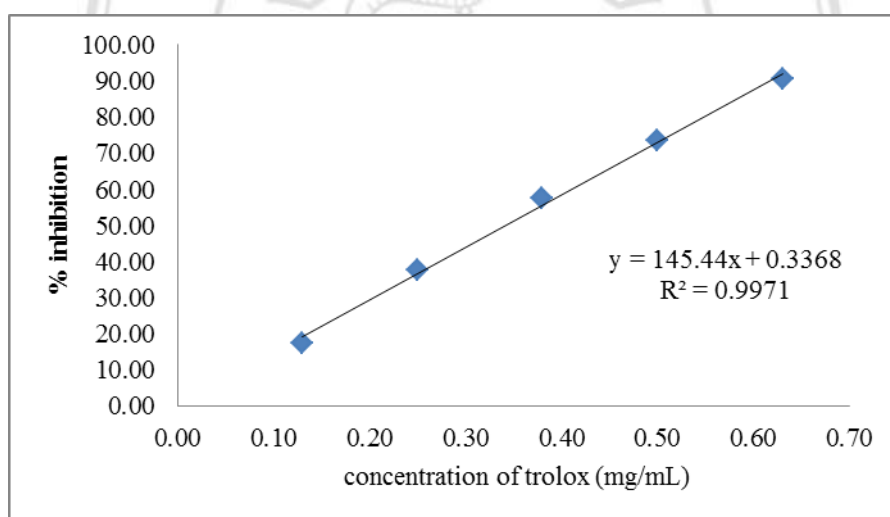


Figure 4.4 Calibration curves of standard trolox solution by ABTS method for the fractions

Table 4.9 The percentage inhibition of ascorbic acid solution by ABTS

Concentration of ascorbic acid (mg/mL)	% inhibition	
	essential oils	fractions
0.09	18.17	15.44
0.18	36.84	36.49
0.26	53.73	54.60
0.35	70.23	74.99
0.44	91.26	90.52

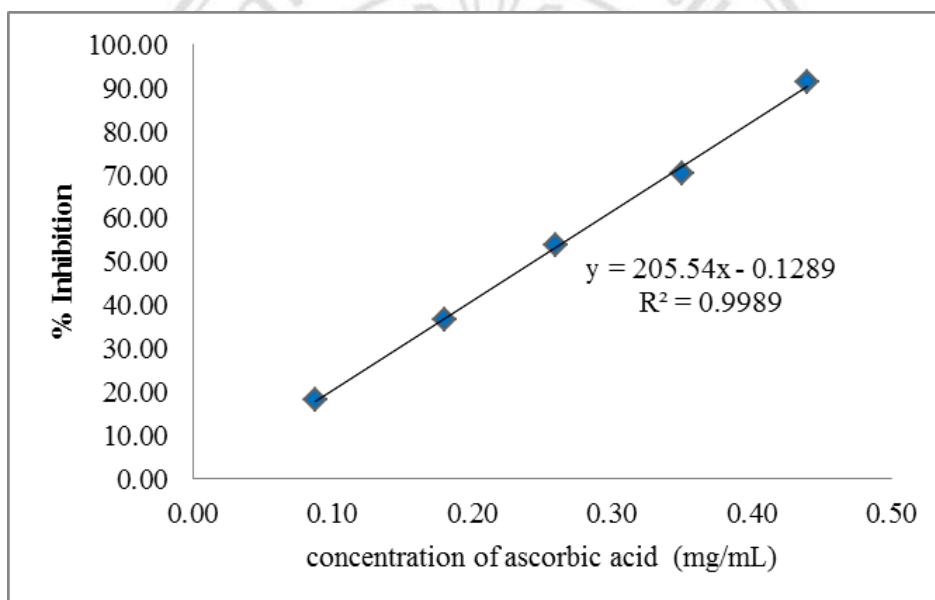


Figure 4.5 Calibration curves of standard ascorbic acid solutions by ABTS method for the essential oils

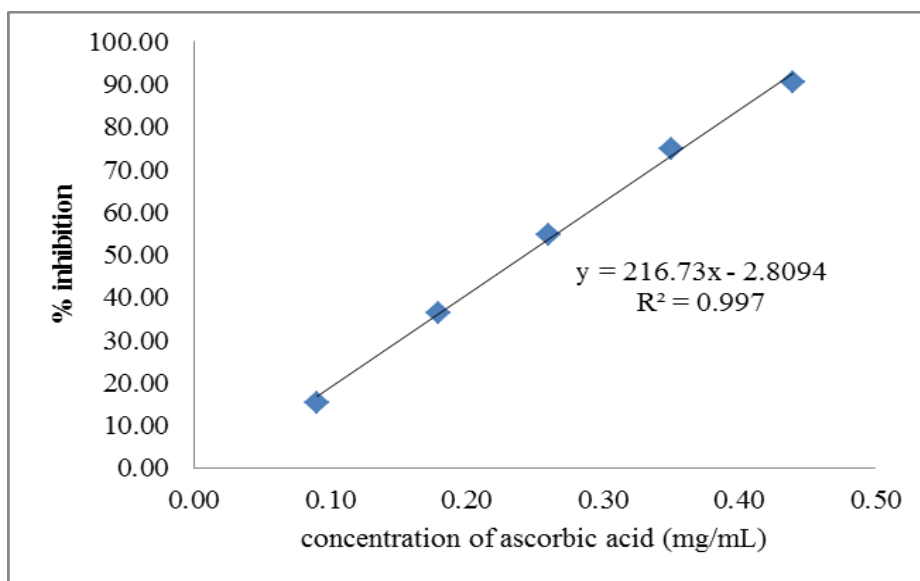


Figure 4.6 Calibration curves of standard ascorbic acid solutions by ABTS method for the fractions

The results are presented in Table 4.10. The antioxidant of each essential oil ([OP1] and [OP3]) was calculated from the calibration curves of trolox and ascorbic acid (the standard curve equations: $y = 148.05x + 0.7928$, $R^2 = 0.9978$ and $y = 205.54x - 0.1289$, $R^2 = 0.9989$, respectively; Figure 4.3 and 4.5) and expressed in the term of mg trolox equivalent antioxidant capacity (TEAC)/g of the extract and mg ascorbic acid equivalent antioxidant capacity (VCEC)/g of the extract, respectively. The essential oil of *G. pictum* [OP1] (10.6 mg/mL) showed trolox and ascorbic acid equivalent antioxidant capacities of 40.12 mg TEAC/g and 29.32 mg VCEC/g extract, respectively, while the essential oil of *G. divaricata* [OP3] (50 mg/mL) had trolox and ascorbic acid equivalent capacities of 5.10 mg TEAC/g and 3.77 mg VCEC/g extract, respectively (Table 4.10). All of the essential oils possessed antioxidant activity. The essential oil of *G. pictum* leaves exhibited a higher antioxidant activity than *G. divaricata* leaves. Phytol, a component of these essential oils, has been reported to possess antioxidant activity (by measuring the cupric ion reducing antioxidant capacity) (146).

Table 4.10 The antioxidant activities of the essential oil [OP1] and the fractions [PP1] of *G. pictum* and the essential oil of *G. divaricata* [OP3] by ABTS assay

Medicinal plant/samples	Trolox	Ascorbic acid
	(mg TEAC /g extract)	(mg VCEC /g extract)
<i>G. pictum</i> leaves		
[OP1]	40.12±0.14	29.32±0.10
[PP1H]	19.63 ± 0.48	13.75 ± 0.32
[PP1EA]	69.19 ± 0.73	48.04 ± 0.49
[PP1B]	29.53 ± 0.16	22.24 ± 0.11
[PP1A]	4.25 ± 0.25	6.48 ± 0.16
<i>G. divaricata</i> leaves		
[OP3]	5.10±0.08	3.77±0.06

The antioxidant of each fraction [PP1] was calculated from the calibration curves of trolox and ascorbic acid (the standard curve equations: $y = 145.44x + 0.3368$, $R^2 = 0.9971$ and $y = 216.73x - 2.8094$, $R^2 = 0.9970$, respectively; Figure 4.4 and 4.6). The results are shown in Table 4.9 and expressed in the term of mg trolox equivalent antioxidant capacity (TEAC)/ g of the extract and mg ascorbic acid equivalent antioxidant capacity (VCEC)/g of the extract, respectively. The different fractions from *G. pictum* leaves; hexane [PP1H], EtOAc [PP1EA], *n*-BuOH [PP1B] and aqueous [PP1A] fractions exhibited significant potential antioxidant activities with the values of 19.63, 69.19, 29.53 and 4.25 mg TEAC/g, respectively and showed with the values of 13.75, 48.04, 22.24 and 6.48 mg VCEC/g, respectively. From these results revealed the antioxidant activities in ABTS assay of four fractions in the order: EtOAc [PP1EA] > *n*-BuOH [PP1B] > hexane [PP1H] > aqueous [PP1A], respectively.

4.6.2. DPPH method

In the DPPH assay, this method depends on the reduction of the purple-colored DPPH radical (DPPH[•]) by accepting an electron or proton radical from the antioxidant to form the reduced form DPPH (DPPH-H). The color changes

from purple to yellow after reduction which can be determined spectrophotometrically at 520 nm. The degree of discoloration indicates the scavenging potential of the antioxidant or sample by their hydrogen donating ability (147).

The antioxidant activities of the extracts [P1] and the fractions [PP1] of *G. pictum* leaves and the extracts of *G. divaricata* [P3] leaves were evaluated using the DPPH assay. A plot of the percentage inhibition of DPPH against the concentration of the sample solutions was prepared and the IC₅₀ values of each crude extract was determined from the calibration curve.

A series of standard solutions containing: 0.01-0.3 mg/mL of trolox and ascorbic acid, were prepared. The percentage inhibition of each concentration of trolox and ascorbic acid are shown in Table 4.11 and their calibration curves are shown in Figure 4.7.

Table 4.11 The percentage inhibition of trolox and ascorbic acid solution by DPPH

Concentration (mg/mL)	% inhibition	
	trolox	Ascorbic acid
0.01	-	7.40
0.02	8.78	13.09
0.04	19.60	33.94
0.06	-	44.28
0.08	39.45	60.69
0.10	49.41	81.77
0.12	62.15	-
0.14	72.48	-
0.18	89.86	-
0.20	92.59	-
0.30	-	99.38

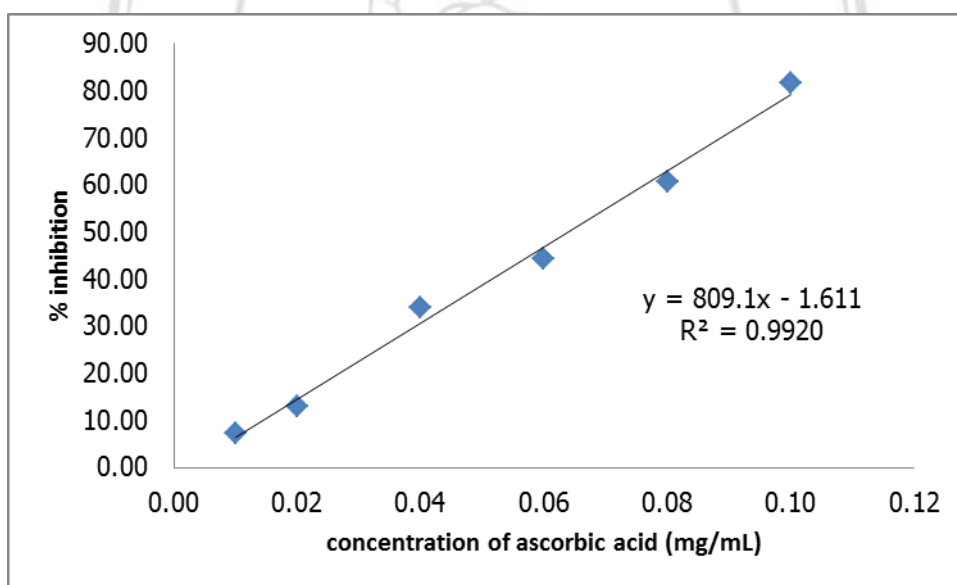
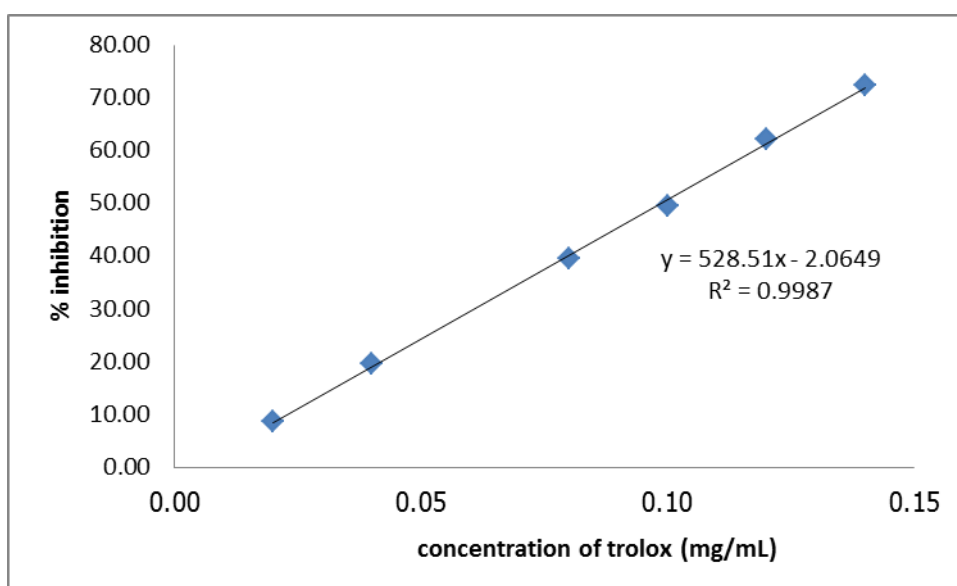


Figure 4.7 Calibration curves for DPPH assay

The inhibitory concentration at 50% (IC_{50}) of each fraction was measured and compared with the antioxidant standard; trolox and ascorbic acid (Table 4.12). The calibration curves of trolox and ascorbic acid (the standard curve equations: $y = 528.51x + 2.0649$, $R^2 = 0.9987$ and $y = 809.1x - 1.611$, $R^2 = 0.9920$, respectively; Figure 4.7) indicated the IC_{50} values of 0.10 and 0.06 mg/mL, respectively.

Table 4.12 The antioxidant activities of the extracts [**P1**] and the fractions [**PP1**] of *G. pictum* and the extracts of *G. divaricata* [**P3**] by DPPH assay

Medicinal plant/samples	IC ₅₀ (mg/mL)
<i>G. pictum</i> leaves	
[P1H]	19.95±0.01
[P1C]	4.41±0.01
[P1E]	5.96±0.01
[P1D]	4.79±0.001
[P1M]	2.05±0.01
[PP1H]	7.60 ± 0.28
[PP1EA]	0.78 ± 0.01
[PP1B]	2.58 ± 0.08
[PP1A]	18.08 ± 0.69
<i>G. divaricata</i> leaves	
[P3H]	5.28 ± 0.01
[P3D]	4.28 ± 0.01
[P3M]	2.87 ± 0.02
Trolox	0.01±0.002
Ascorbic acid	0.06±0.003

For *G. pictum*, the MeOH extract [**P1M**] showed the highest antioxidant activity with an IC₅₀ value of 2.05 mg/mL followed by the CHCl₃ [**P1C**], the CH₂Cl₂ [**P1D**], the EtOH [**P1E**] and the hexane [**P1H**] extracts with IC₅₀ values of 4.41, 4.79, 5.96, 19.95 mg/mL, respectively (Table 4.12). In addition, the hexane [**PP1H**], EtOAc [**PP1EA**], *n*-BuOH [**PP1B**] and aqueous [**PP1A**] fractions showed significant antioxidant activities with IC₅₀ values of 7.60, 0.78, 2.58 and 18.08 mg/mL, respectively (Table 4.12). These results showed that the EtOAc [**PP1EA**] fraction showed the highest antioxidant activity with the lowest IC₅₀ value followed by the *n*-BuOH [**PP1B**], hexane [**PP1H**] and aqueous [**PP1A**] fractions, respectively which correlated to the results of the ABTS assay.

For *G. divaricata*, the MeOH extract [P3M] possessed the highest antioxidant activity with an IC₅₀ of 2.87 mg/mL. The hexane [P3H] and CH₂Cl₂ [P3D] extracts also showed antioxidant activity with IC₅₀ values of 5.28 and 4.28 mg/mL, respectively (Table 4.12). The EtOH extract of *G. divaricata* leaves was reported to have significant antioxidant properties (79) and these studies reported here support these earlier observations. This activity may be due to the presence of phenolic and flavonoid compounds which have significant correlations with the total antioxidant activity and free radical-scavenging capacities (80).

4.6.3. Total phenolic and total flavonoid contents

The total phenolic content was measured a spectrophotometrically method using the Folin-Ciocalteu's reagent. The principle of this method is the reduction of Folin-Ciocalteu's reagent by phenols under basic condition to form a blue chromophore consisted of a phosphotungstic-phosphomolybdenum complex. This chromophore can be quantified by UV-vis spectrophotometry (145). Table 4.13 showed the total phenolic contents in various fractions are expressed in the term of mg gallic acid equivalent (GAE) /g of the extract (the standard curve equation: $y = 10.802x + 0.0447$, $R^2 = 0.9919$; Figure 4.8).

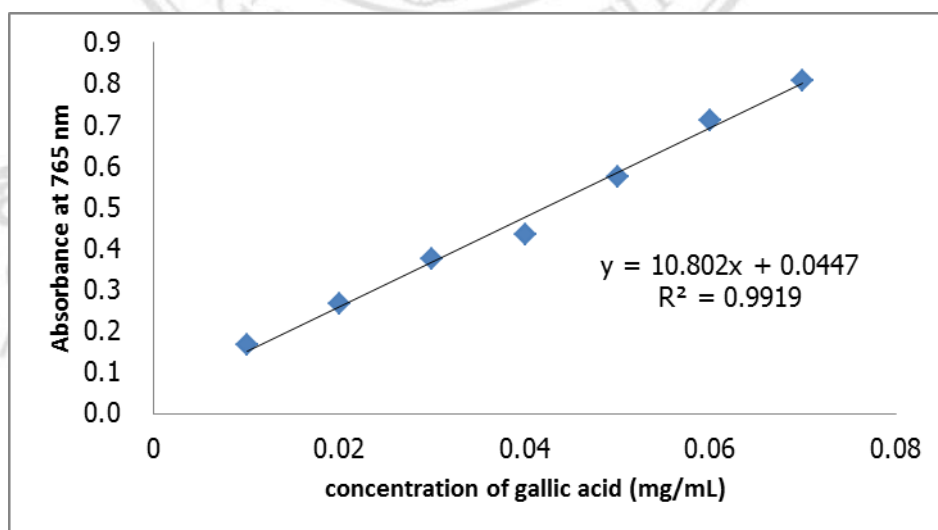


Figure 4.8 Calibration plot for phenolic determination

The total phenolic contents ranged from 11.69 - 102.57 mg GAE/g for the extract. The EtOAc fraction [PP1EA] showed the highest total phenolic

content (102.57 mg GAE/g) followed by the *n*-BuOH fraction [PP1B] (45.33 mg GAE/g) and the aqueous fraction [PP1A] (16.51 GAE/g), whereas the hexane fraction [PP1H] had the lowest total phenolic content (11.69 mg GAE/g) (Table 4.13).

Table 4.13 The percentage yield, total phenolic and flavonoid contents of different fractions of *G. pictum* leaves

Fractions	Total phenolic contents	Total flavonoid contents
	(mg GAE/g extract) ^a	(mg QE/g extract) ^b
[PP1H]	11.69 ± 0.09	28.21 ± 0.04
[PP1EA]	102.57 ± 0.19	22.45 ± 0.02
[PP1B]	45.33 ± 0.23	9.02 ± 0.04
[PP1A]	16.51 ± 0.16	2.02 ± 0.02

^aGAE: gallic acid equivalent, ^bQE: quercetin equivalent, Values are expressed as means of triplicate determinations ± SD.

Flavonoids are natural constituents of plants which have potential biological activities including antioxidant properties. The determination of total flavonoid contents was measured spectrophotometrically using aluminium chloride. This method is based on the formation of an acid stable complex between the flavonoid and aluminium chloride which has a maximum absorption at 415 nm (147). The total flavonoid contents of all fractions are summarized in Table 4.14 which are expressed in terms of mg quercetin equivalent (QE)/g of the extract (the standard curve equation: $y = 26.916x - 0.0287$, $R^2 = 0.9990$; Figure 4.9).

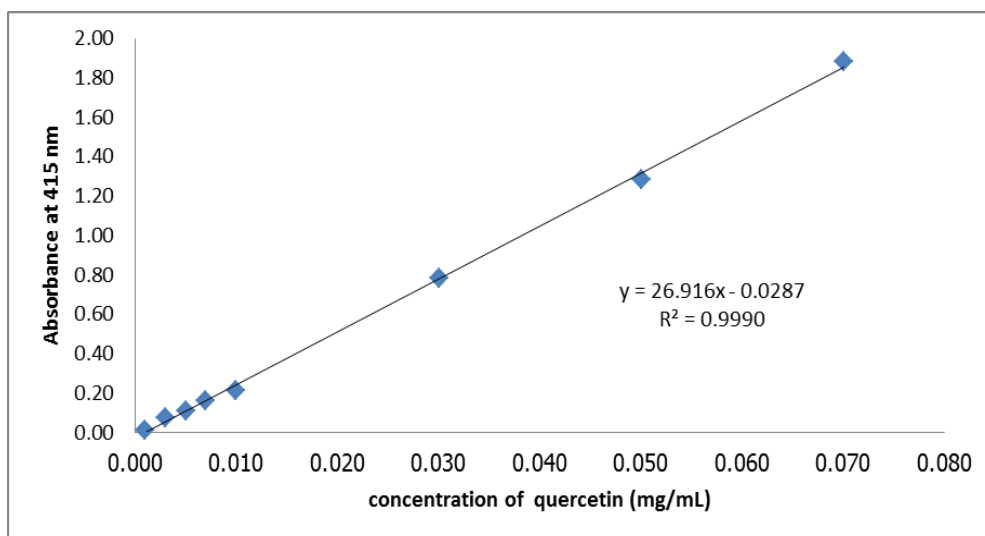


Figure 4.9 Calibration plot for flavonoid determination

The total flavonoid contents of *G. pictum* fractions ranged from 2.02 - 28.21 mg QE/g of the extract. The highest total flavonoid content found in the hexane fraction [PP1H] (28.21 mg QE/g) followed by the EtOAc fraction [PP1EA] (22.45 mg QE/g) and the *n*-BuOH fraction [PP1B] (9.02 mg QE/g), and the lowest total flavonoid contents was shown in the aqueous fraction [PP1A] (2.02 mg QE/g) (Table 4.13).

4.7. Preliminary phytochemical screening for the fractions of *G. pictum* [PP1]

The preliminary phytochemical screening for the secondary metabolites in different fractions of *G. pictum* leaves in various solvents was performed using standard procedures. The results indicated that *G. pictum* leaves consisted of the flavonoids, steroids, tannins, coumarins, saponins, anthraquinones, phenolics and sugars as shown in Table 4.14. The presence of flavonoids was according to the result described by Ozaki et al. (31).

Table 4.14 Preliminary phytochemical screening of *G. pictum* leave extracts using the standard procedures

Test	Results*
Flavonoids (in 80% EtOH)	+
Steroids (in CHCl ₃)	+
Tannins (in 80% EtOH)	+
Resins (in EtOH)	-
Coumarins (react with 20% NaOH coated filtered paper)	+
Saponins (in water)	+
Anthraquinones (in methanol)	+
Glycosides (in 50% MeOH in the presence of 10% lead acetate)	-
Phenolics (in dichloromethane)	+
Sugars (in water)	+
Alkaloids (in 80% EtOH)	-

*(+): presence, (-): absence of phytochemical.

4.8. Analysis of the hexane fraction of *G. pictum* [PP1H] and the CHCl₃ extract of *S. spirale* [P2C]

The hexane fraction [PP1H] of the leaves of *G. pictum* [PP1] showed anticancer activity against MCF-7 breast cancer cell with an IC₅₀ value of 38.66 µg/mL (Table 4.5). From the previous study of Keawsa-ard (114) reported that the CHCl₃ extract of the leaves of *S. spirale* showed moderately anti-herpes simplex virus type-1 (HSV-1) activity. These fractions were selected to analyze using GC-MS.

4.8.1. Analysis of the hexane fraction of *G. pictum* [PP1H]

The hexane fraction [PP1H] of *G. pictum* was analyzed on an Agilent HP 6890 coupled with a Hewlett-Packard 5973 mass selective detector. The components of the [PP1H] were identified by comparison of their mass spectra from libraries (Wiley7n.l and W8N05ST.L) and by their retention indices (RI) relative to spiked *n*-alkane (C₇-C₃₀) indices on an AT-5MS column with comparisons made with the literature data (Table 4.15). In total, 15 compounds were identified (Figure 4.10), corresponding to 99.4% of of the chromatographical

fraction of the [PP1H] that consisted mainly of triterpene (23.8%) followed by oxygenated acyclic diterpene (18.3%), diterpene (13.4%), esters (12.3%), hydrocarbons (7.4%), carboxylic acid (7.1%), fatty acid (2.6%) and aldehyde (1.1%). Five components, collectively accounting for 13.4% of the total chromatographical fraction, could not be identified due to their relatively low abundance and/or lack of reference spectra. The major compounds were squalene (23.8%), phytol (18.3%) and neophytadiene (13.4%).

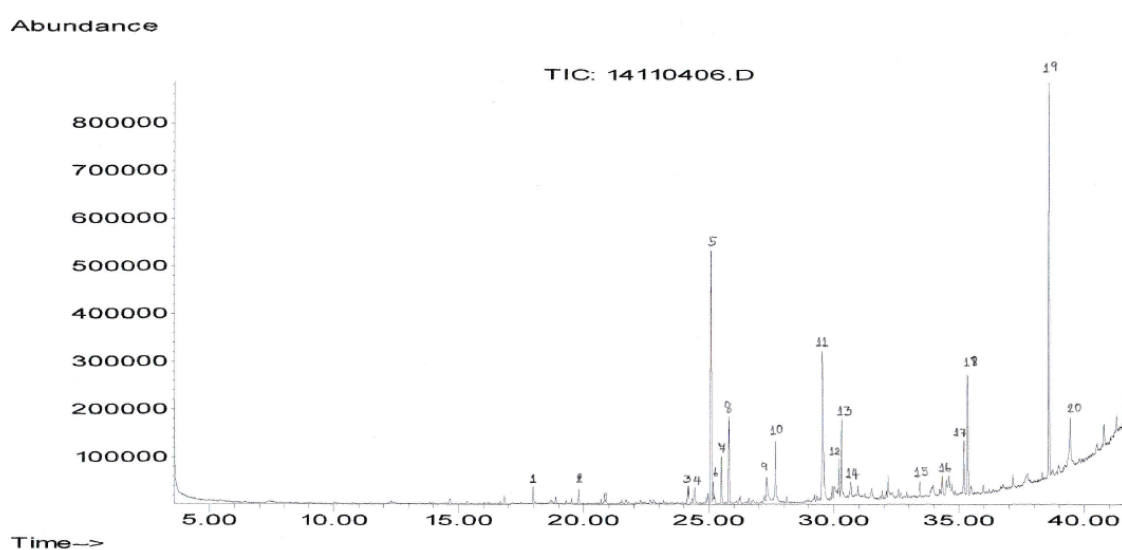


Figure 4.10 Gas chromatogram of the hexane fraction of *G. pictum* leaves [PP1H]

Table 4.15 Chemical constituents of the hexane fraction from the leaves of *G. pictum* [PP1H]

Peak	Compounds	RA ^a (%)	RI (exp) ^b	RI (lit) ^c	Identification ^d	Ref
1	6-Benzofuran carboxaldehyde	1.1	1452.8	-	MS	-
2	Unidentified	1.0	1543.9	-	-	-
3	Benzyl benzoate	1.1	1780	1775	RI, MS	116
4	<i>n</i> -Octadecane	1.4	1800	1800	RI, MS	94
5	Neophytadiene	13.4	1835	1838	RI, MS	55
6	(2E)-3,7,11,15- Tetramethyl-2-hexadecene	0.9	1840	-	MS	-

Table 4.15 (continued)

Peak	Compounds	RA ^a (%)	RI (exp) ^b	RI (lit) ^c	Identification ^d	Ref
7	Unidentified	2.5	1859	-	-	-
8	Unidentified	4.7	1877	-	-	-
9	Hexadecanoic acid	2.6	1976	1972	RI, MS	115
10	Ethyl hexadecanoate	3.5	2000	2000	RI, MS	117
11	Phytol	18.3	2115.1	2112	RI, MS	96
12	Ethyl linoleate	2.0	2161	2159	RI, MS	118
13	Ethyl linolenate	4.5	2168	2169	RI, MS	118
14	Ethyl decanoate	1.2	2193	2194	RI, MS	96
15	<i>n</i> -Tetracosane	0.9	2400	2400	RI, MS	94
16	Unidentified	1.1	2462	-	-	-
17	Unidentified	4.1	2531	-	-	-
18	1,2-Benzenedicarboxylic acid	7.1	2543	-	MS	-
19	Squalene	23.8	2817	2820	RI, MS	55
20	<i>n</i> -Nonacosane	4.2	2900	2900	RI, MS	94
	Aldehyde	1.1				
	Esters	12.3				
	Hydrocarbons	7.4				
	Diterpene	13.4				
	Fatty acid	2.6				
	Oxygenated acyclic diterpene	18.3				
	Carboxylic acid	7.1				
	Triterpene	23.8				
	Unidentified (5 in total)	13.4				
	Oil components (total)	99.4				

^aRA: relative area (peak area relative to total peak area); ^bRI(exp): retention indices relative to *n*-alkanes (C₇-C₃₀) on AT-5MS column; ^cRI(lit): retention indices from literature data; ^dMS: from a comparison of the mass spectrum with MS libraries and RI of literature.

Squalene, a major component of **[PP2H]**, is one of the triterpene intermediates in the endogenous synthesis pathway of cholesterol. The interesting biological activities of squalene have been reported. In animal model studies, squalene was found to be a chemoprotective agent. It showed significant inhibitory effects against colon, lung and skin carcinogenesis (148). Squalene also had antioxidant activity (149-151). The recent study of squalene showed the cytotoxic activity against mouse melanocyte (B16-F10) and human macrophage (U937) cells with EC₅₀ values of more than 100 μM (152). The anticancer and antioxidant activities of the hexane fraction **[PP2H]** of *G. pictum* may be due to the biological activities of squalene.

Neophytadiene, another major component, is in a diterpene group which has various biological activities such as antimicrobial, antioxidant, anti-inflammatory and antipyretic. Moreover, neophytadiene was also involved in an inflammatory reduction as a competitive inhibitor of lipoxygenase or cyclooxygenase (153-154). In this study, the hexane fraction of *G. pictum* **[PP1H]** had no antibacterial activity against the tested bacteria, while neophytadiene showed antimicrobial activity. It may suggest that the lower concentration of the tested fraction **[PP1H]** or the other components of **[PP1H]** inhibit or mask the antimicrobial activity of neophytadiene.

4.8.2. Analysis of the CHCl₃ extract of *S. spirale* [P2C]

The CHCl₃ extract **[P2C]** of *S. spirale* was analyzed on an Agilent HP 6890 coupled with a Hewlett-Packard 5973 mass selective detector. The components of the **[P2C]** were identified by comparison of their mass spectra from libraries (Wiley7n.l and W8N05ST.L) and by their retention indices (RI) relative to spiked *n*-alkane (C₇-C₃₀) indices on an AT-5MS column with literature data (Table 4.16). In total, 26 compounds were identified (Figure 4.11), corresponding to 99.1% of the chromatographical fraction of **[P2C]** which consisted mainly of esters (34.6%) followed by hydrocarbons (20.9%), diterpene (7.4%), oxygenated acyclic diterpene (5.6%), fatty acid (4.3%), monoterpene lactone (2.2%), isoprenoid (2.1%), oxygenated sesquiterpene (1.8%), and terpene

lactone (0.8%). Seven components, collectively accounting for 19.4% of the total chromatographical extract, could not be identified due to their relatively low abundance and/or lack of reference spectra. The major compounds were triacetin (16.1%), neophytadiene (7.4%) and ethyl hexadecanoate (6.3%).

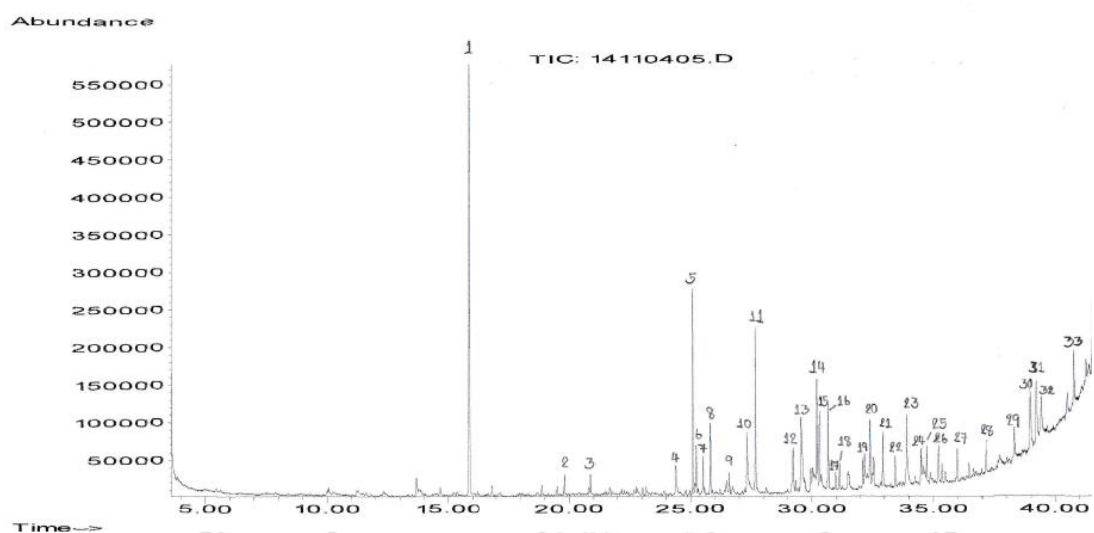


Figure 4.11 Gas chromatogram of the CHCl₃ extract of *S. spirale* stems [P2C]

Table 4.16 Chemical constituents of the CHCl₃ extract from the stems of *S. spirale* [P2C]

Peak	Compounds	RA ^a (%)	RI (exp) ^b	RI (lit) ^c	Identification ^d	Ref
1	Triacetin	16.1	1353	1344	RI, MS	119
2	Dihydroactinidiolide	0.8	1544	1542	RI, MS	120
3	Diethyl phthalate	0.3	1596	1594	RI, MS	121
4	(-)-Loliolide	2.2	1794	1800	RI, MS	122
5	Neophytadiene	7.4	1834	1838	RI, MS	55
6	Hexahydrofarnesyl acetone	1.8	1843	1845	RI, MS	93
7	Unidentified	1.4	1859	-	-	-
8	Unidentified	2.6	1877	-	-	-
9	Methyl hexadecanoate	0.9	1925	1926	RI, MS	96
10	Hexadecanoic acid	4.3	1971	1972	RI, MS	115

Table 4.16 (continued)

Peak	Compounds	RA^a (%)	RI (exp)^b	RI (lit)^c	Identification^d	Ref
11	Ethyl hexadecanoate	6.3	1993	1994	RI, MS	96
12	<i>n</i> -Heneicosane	2.7	2100	2100	RI, MS	94
13	Phytol	5.6	2116	2112	RI, MS	96
14	Ethyl linoleate	4.3	2161	2159	RI, MS	46
15	Ethyl linolenate	2.9	2168	2169	RI, MS	46
16	Ethyl octadecanoate	3.8	2193	2193	RI, MS	46
17	Unidentified	0.7	2214	-	-	-
18	Bicyclo[10.8.0]eicosane, cis-	1.0	2226	-	MS	-
19	<i>n</i> -Tricosane	1.1	2300	2300	RI, MS	94
20	Unidentified	3.1	2317	-	-	-
21	4,8,12,16- Tetramethylheptadecan-4- olide	2.1	2354	-	MS	-
22	<i>n</i> -Tetracosane	1.4	2400	2400	RI, MS	94
23	1,21-Docosadiene	4.7	2429	-	MS	-
24	Unidentified	1.2	2475	-	-	-
25	<i>n</i> -Pentacosane	1.3	2500	2500	RI, MS	94
26	Unidentified	1.5	2532	-	-	-
27	<i>n</i> -Hexacosane	1.4	2600	2600	RI, MS	94
28	<i>n</i> -Heptacosane	1.5	2700	2700	RI, MS	94
29	<i>n</i> -Octacosane	1.7	2800	2800	RI, MS	94
30	Unidentified	4.3	2851	-	-	-
31	Unidentified	4.6	2874	-	-	-
32	<i>n</i> -Nonacosane	2.7	2900	2900	RI, MS	94
33	<i>n</i> -Triacontane	1.4	3000	3000	RI, MS	94
Esters		34.6				
Terpene lactone		0.8				
Monoterpene lactone		2.2				

Table 4.16 (continued)

Peak	Compounds	RA ^a (%)	RI (exp) ^b	RI (lit) ^c	Identification ^d	Ref
	Diterpene	7.4				
	Oxygenated sesquiterpene	1.8				
	Fatty acid	4.3				
	Hydrocarbons	20.9				
	Oxygenated acyclic diterpene	5.6				
	Isoprenoid	2.1				
	Unidentified (7 in total)	19.4				
	Oil components (total)	99.1				

^aRA: relative area (peak area relative to total peak area); ^bRI(exp): retention indices relative to *n*-alkanes (C₇-C₃₀) on AT-5MS column; ^cRI(lit): retention indices from literature data; ^dMS: from a comparison of the mass spectrum with MS libraries and RI of literature.

The major component, triacetin, is an ester which was known as glyceryl acetate. It is used in cigarette filters manufacturing for the solidification of acetyl cellulose. In the food industry, it is used as a plasticizer for chewing gum and a food additive. In pharmaceuticals, it is used in the production of capsules and tablets, and used as a humectant. Moreover, it is added in gasoline for antiknocking of the engine and adjusts the cold and viscosity properties of biodiesel. Triacetin is also used as an additive in the cosmetic and perfume industries (155-157).

Ethyl hexadecanoate or ethyl palmitate, another major component, is the natural fatty acid ester which showed cytotoxicity against macrophages and blocks the reticuloendothelial system. It also exhibited significant anti-inflammatory activities in various rat models by reducing rat paw edema, prostaglandin E2 (PGE2) content in inflammatory exudates, plasma tumor necrosis factor- α (TNF- α) and interleukin-6 (IL-6) levels, NF- κ B expression in liver and lung tissue and ameliorating histopathological changes. Topical of ethyl palmitate decreased myeloperoxidase (MPO) activity in an ear edema model.

From these interesting results, ethyl palmitate was chosen for further drug investigation (158).

In addition, ethyl linoleate, another fatty acid ester, also showed anti-inflammatory effects (159) and has a water-holding lipid property which was used in topical postburn treatment (160). Ethyl linolenate was used as a supplementation for treatment of α -linolenic acid deficiency (ALAD) (161). (-)-Loliolide showed cytostatic activity against human KB carcinoma and murin P388 lymphocytic cells with ED₅₀ values of 10 and 3.5-22 μ g/kg (162), possessed antioxidant activity and exhibited a cell protective effect against H₂O₂ induced cell damage (163).

4.9. Isolation and purification of the essential oil of *G. divaricata* [OP3]

The essential oil of the leaves of *G. divaricata* [OP3] showed moderate activity against KB (oral cavity cancer), MCF-7 (breast cancer) and NCI-H187 (small cell lung cancer) cell lines (Table 4.4) and also had an antimycobacterial activity against *Mycobacterium tuberculosis* H₃₇Ra (Table 4.5). Therefore, this oil was selected for further purification.

The essential oil ([OP3], 72.3 mg) was subjected to normal phase column chromatography using a gradient of EtOAc in petroleum ether (1:99 to 100:0) as eluent to afford 17 fractions (Scheme 3.7). All fractions were identified using an NMR spectrometer in solutions of CDCl₃ with TMS as an internal standard. [OP3-4] (9.0 mg) and [OP3-6] (1.6 mg) were obtained as colourless oils and showed clear ¹H-NMR spectra and were further identified using GC-MS.

The ¹H NMR (500 MHz) spectrum of compound [OP3-4] (Appendix A Figure 1, page 266) exhibited signals for three methyl groups as doublets at δ 0.96, 0.87 and 0.80. An olefinic proton signal was found as a doublet at δ 5.45 (d, J = 5.0 Hz). The broad singlet resonance at δ 1.70 indicated an allylic methyl proton. GC-MS analysis of [OP3-4] was also matched with cubenol (Figure 4.12). From these data, the structure of this compound was assigned as cubenol by the above evidences and by comparisons with the previously published spectral data (129) (Table 4.17).

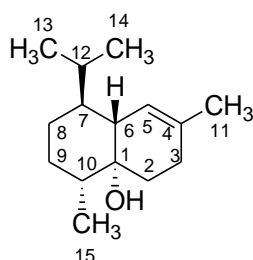


Figure 4.12 Chemical structure of compound [OP3-4] (cubenol)

Table 4.17 Comparison of NMR spectroscopic data of compound [OP3-4]

Position	δ_{exp} (500 MHz, CDCl ₃)	δ_{lit} (300.13 MHz, CDCl ₃) (129)
	¹ H (mult, <i>J</i> (Hz))	¹ H (mult, <i>J</i> (Hz))
1	-	-
2a	1.30 (1H, m)	1.35 (1H, m)
2b	2.03 (1H, m)	2.03 (1H, m)
3a	2.13 (1H, m)	2.15 (1H, m)
3b	2.08 (1H, m)	2.05 (1H, m)
4	-	-
5	5.45 (1H, d, <i>J</i> = 4.0)	-
6	1.93 (1H, m)	1.84 (1H, br, d, <i>J</i> = 12.1)
7	1.55 (1H, m)	1.50 (1H, m)
8a	1.08 (1H, m)	1.04 (1H, m)
8b	1.60 (1H, m)	1.63 (1H, dddd, <i>J</i> = 3.4, 3.4, 3.4, 12.6)
9a	1.54 (1H, m)	1.41 (1H, m)
9b	1.54 (1H, m)	1.41 (1H, m)
10	1.25 (1H, m)	1.31 (1H, m)
11	1.70 (3H, m)	1.71 (3H, br,s)
12	2.10 (1H, m)	2.09 (1H, m)
13	0.87 (3H, d, <i>J</i> = 6.5)	0.91 (3H, d, <i>J</i> = 7.0)
14	0.80 (3H, d, <i>J</i> = 7.0)	0.73 (3H, d, <i>J</i> = 7.0)
15	0.96 (3H, d, <i>J</i> = 6.0)	0.93 (3H, d, <i>J</i> = 6.6)

The ¹H NMR (500 MHz) spectrum of compound [OP3-6] (Appendix A Figure 2, page 266) indicated singlet resonances for three methyl groups at δ 1.04, 1.06 and

1.28 and resonances for exocyclic methylene protons at δ 4.67 and 4.69 and two methine protons at δ 0.46 and 0.48. The GC-MS of [**1H-3.1**] matched with spathulenol (Figure 4.13).

From these data, the structure of this compound was assigned as spathulenol by the above evidences and by the comparison with previously published NMR spectroscopic data (128) (Table 4.18).

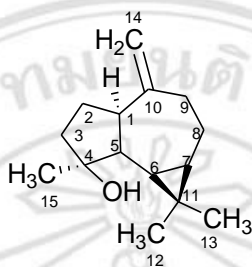


Figure 4.13 Chemical structure of compound [**OP3-6**] (spathulenol)

Table 4.18 Comparison of NMR spectroscopic data of compound [**OP3-6**]

Position	δ_{exp} (500 MHz, CDCl_3)	δ_{lit} (200 MHz, CDCl_3) (128)
	^1H (mult, J (Hz))	^1H (mult, J (Hz))
1	a	-
2	a	-
3	a	-
4	-	-
5	a	-
6	0.46 (d, $J = 9.4$, 1H)	0.45 (d, $J = 9.0$, 1H)
7	0.48 (d, $J = 9.6$, 1H)	0.47 (d, $J = 9.0$, 1H)
8	a	-
9	a	-
10	-	-
11	-	-
12	1.06 (s, 3H)	1.04 (s, 3H)
13	1.04 (s, 3H)	1.05 (s, 3H)
14	4.69 (s, 1H), 4.67 (s, 1H)	4.67 (d, $J = 5.0$, 2H)
15	1.28 (s, 3H)	1.28 (s, 3H)

^aSignals for these protons were overlapped with those of others and therefore these assignments could not be determined.

The cytotoxic activities of these two major components were determined against KB, MCF-7 and NCI-H187 cell lines. They were also tested for antimycobacterial activities. The results are shown in Table 4.19.

Table 4.19 The cytotoxicity and antimycobacterial activity of compounds [OP3-4] and [OP3-6]

Samples	Cytotoxicity			Antimycobacterial activity
	IC ₅₀ ^a (µg/mL)			<i>M. tuberculosis</i> H ₃₇ Ra
	KB	MCF-7	NCI-H187	MIC ^b (µg/mL)
[OP3-4]	NA	NA	45.37 ± 2.94	NA
[OP3-6]	NA	NA	NA	NA
Ellipticine ^c	0.440±0.089	-	0.858±0.43	-
Doxorubicin ^c	0.610±0.194	9.16±0.391	0.095±0.017	-
Tamoxifen ^c	-	4.94±0.837	-	-
Rifampicin ^d	-	-	-	0.003-0.025
Streptomycin ^d	-	-	-	0.156-0.313
Isoniazid ^d	-	-	-	0.023-0.046
Ofloxacin ^d	-	-	-	0.391-0.781
Ethambutol ^d	-	-	-	0.234-0.469

^aConcentration that killed 50% of cell lines; ^bMinimum inhibitory concentration; ^cAnticancer drugs used as positive control; ^dAntimycobacterial drugs used as positive controls; NA = no activity.

The [OP3-4] (cubenol) showed cytotoxicity only against NCI-H187 cells with an IC₅₀ value of 45.37 µg/mL, while [OP3-6] (spathulenol) was inactive against all cancer cell lines (Table 4.19). From Table 4.4, the essential oil [OP3] exhibited cytotoxicity against the NCI-H187 cell lines with the IC₅₀ values of 17.65 µg/mL. Cubenol was found as a major component in this essential oil [OP3] (Table 4.3). Therefore, cubenol may be responsible for the cytotoxic activity of the [OP3]. Moreover, the assay of [OP3-4] (cubenol) and [OP3-6] (spathulenol) against

Mycobacterium tuberculosis H37Ra indicated that these compounds were inactive in this assay (Table 4.19).

4.10. Isolation and purification of the fractions of *G. pictum* [PP1]

4.10.1. Isolation and purification of the hexane fraction of *G. pictum* [PP1H]

The hexane fraction [PP1H] from the liquid-liquid extraction of the leaves of *G. pictum* [PP1] showed anticancer activity against MCF-7 (breast cancer cell line) with IC₅₀ values of 38.66 µg/mL (Table 4.4). Therefore, this fraction was selected for further purification.

The hexane fraction of *G. pictum* ([PP1H], 1.1 g) was subjected to normal phase column chromatography, using a gradient of hexane and EtOAc (100:0 to 0:100) followed by EtOAc and MeOH (50:50 to 0:100) as eluent to afford 13 fractions (Scheme 3.8). Fraction [1H-3] showed one major compound, while fraction [1H-9] exhibited crystals mixed with a green paste. Therefore, fractions [1H-3] and [1H-9] were selected for further purification.

4.10.1.1. Isolation and purification of [1H-3]

Fraction [1H-3] (6.6 mg) was purified by preparative TLC using hexane as the eluent to obtain [1H-3.1] and [1H-3.2] (Scheme 3.9).

Compound [1H-3.1] was obtained as a yellow oil (2.0 mg). It was identified by NMR spectroscopy. The ¹H-NMR (500 MHz) spectrum of [1H-3.1] (Appendix A Figure 3, page 267) indicated an unsaturated hydrocarbon. The spectrum exhibited signals for the six olefinic protons at δ 5.15-5.09 (m, 6H). A broad multiplet at δ 2.09-1.96 (m, 20H) indicated ten methylene groups. Resonances for eight methyl groups were found at δ 1.68-1.60 (s, 8x3H). GC-MS and mass spectrometry was used to identify and confirm the identity of this compound. The LR-ESIMS mass spectrum showed the molecular ion peak at *m/z* 410 [M⁺] which corresponded to the molecular formula C₃₀H₅₀. The GC-MS of [1H-3.1] matched with squalene (Figure 4.14)

From these data, the structure of compound [1H-3.1] was identified as squalene (Figure 4.14) by the above evidences and from comparisons with previously published spectroscopic data (149) (Table 4.20).

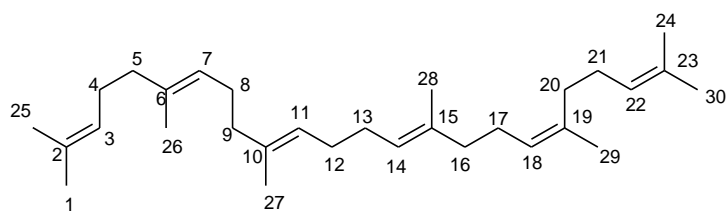


Figure 4.14 Chemical structure of compound [1H-3.1] (squalene)

Table 4.20 Comparison of NMR spectroscopic data of compound [1H-3.1]

Signal	δ_{exp} (500 MHz, CDCl ₃)	δ_{lit} (500 MHz, CDCl ₃) (149)
	¹ H (mult, J (Hz))	¹ H (mult, J (Hz))
1	5.15-5.09 (m, 6H)	5.14-5.07
2	2.09-1.96 (m, 20H)	2.06-1.98
3	1.68-1.60 (m, 24H)	1.68-1.55

Squalene has been reported for its anticancer and antioxidant activity, and is also found as a major component in the human sebum oil. Squalene plays a role as a skin emollient, and hydration and repairing and renewing aging skin. Therefore, squalene has been used as an ingredient in cosmetic formulations. In pharmaceutical applications, squalene has also been used as a lipid emulsion as a vaccine adjuvant. Moreover, the studies of the consumption of squalene showed significant decreases in the levels of total cholesterol, LDL-cholesterol and triacylglyceride in hypercholesterolemia patients as well as the reduction in wrinkles in human skin (149-151).

4.10.1.2. Isolation and purification of [1H-9]

Fraction [1H-9] (93.2 mg), which consisted of crystals mixed with a green paste, was subjected to normal phase column chromatography, using a gradient of hexane and EtOAc (100:0 to 0:100) as eluent to afford 13 fractions (Scheme 3.10).

Fraction [1H-9.6] showed impure crystals (eluent system: hexane /EtOAc 80:20). Recrystallizations of [1H-9.6] from hexane afforded white crystalline needles (9.6 mg) which were further identified by NMR spectroscopy. The LR-ESIMS mass spectrum showed the molecular ion peak at m/z 413 [$M+H^+$] which corresponded to the molecular formula

C₂₉H₄₈O. The ¹H NMR (500 MHz) spectrum of compound [1H-9.6] (Appendix A Figure 4, page 267) exhibited signals for three olefinic methine protons. The singlet resonance at δ 5.35 was characteristic of an endocyclic double bond between C-5 and C-6. The two doublet of doublets at δ 5.15 (dd, *J* = 9.0, 15.0 Hz, 1H, H-22) and 5.02 (dd, *J* = 9.0, 15.0 Hz, 1H, H-23) were characteristic signals for exocyclic double bond at C-22 and C-23. Six methyl proton resonances were also observed. Two singlet methyl protons exhibited signals at δ 1.01 (s, 3H, H-19), 0.69 (s, 3H, H-18); three doublet methyl protons exhibited signals at δ 1.02 (d, *J* = 7.0 Hz, 3H, H-21), δ 0.84 (d, *J* = 8.0 Hz, 3H, H-26), δ 0.82 (d, *J* = 5.3 Hz, 3H, H-27) and one triplet methyl signal appeared at δ 0.80 (t, *J* = 7.8 Hz, 3H, H-29). A multiplet at δ 3.52 was assigned to the proton at C-3 which is attached to hydroxyl group.

From these data, the structure of compound [1H-9.6] was identified as stigmasterol (Figure 4.15) by the above evidences and from comparisons with previously published spectral data (164) (Table 4.21).

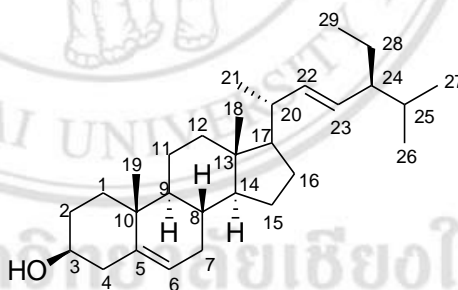


Figure 4.15 Chemical structure of compound [1H-9.6] (stigmasterol)

Table 4.21 Comparison of NMR spectroscopic data of compound [1H-9.6]

Position	δ_{exp} (500 MHz, CDCl ₃)	δ_{lit} (500 MHz, CDCl ₃) (164)
	¹ H (mult, <i>J</i> (Hz))	¹ H (mult, <i>J</i> (Hz))
1	a	-
2	a	-
3	3.52 (m, 1H)	3.51 (m, 1H)
4	a	-
5	-	-
6	5.35 (s, 1H)	5.34 (s, 1H)
7	a	-
8	a	-
9	a	-
10	-	-
11	a	-
12	a	-
13	-	-
14	a	-
15	a	-
16	a	-
17	a	-
18	0.69 (s, 3H)	0.70 (s, 3H)
19	1.01 (s, 3H)	1.01 (s, 3H)
20	-	-
21	1.02 (d, <i>J</i> = 7.0, 3H)	1.03 (d, 3H)
22	5.15 (dd, <i>J</i> = 9.0, 15.0, 1H)	5.17 (dd, <i>J</i> _{22,23} = 15.2, 1H)
23	5.02 (dd, <i>J</i> = 9.0, 15.0, 1H)	5.04 (dd, <i>J</i> _{23,24} = 8.6, 1H)
24	a	-
25	a	-
26	0.84 (d, <i>J</i> = 8.0, 3H)	0.85 (d, 3H)
27	0.82 (d, <i>J</i> = 5.3, 3H)	0.80 (d, 3H)
28	a	-

Table 4.21 (continued)

Position	δ_{exp} (500 MHz, CDCl ₃)	δ_{lit} (500 MHz, CDCl ₃) (164)
	¹ H (mult, <i>J</i> (Hz))	¹ H (mult, <i>J</i> (Hz))
29	0.80 (t, <i>J</i> = 7.8, 3H)	0.81 (t, 3H)

^aSignals for these protons were overlapped with those of others and therefore these assignments could not be determined.

Stigmasterol is one of the phytosterols which is isolated from various plants; for example, *Spilanthes acmella* (165), *Mesua beccariana* (166) and *Bacopa monnieri* Linn (167). The biological activities of stigmasterol have been reported. Stigmasterol, isolated from the leaves of *Spilanthes acmella*, showed moderate antibacterial activity against various bacteria and fungi (165). Whereas, stigmasterol from the aerial part of this plant had MIC values of 12.5 µg/mL against these clinical microbes; *S. aureus*, *Streptococcus pyrogens*, *B. subtilis*, *E. coli*, *Proteus vulgaris*, *S. typhi*, *S. dysenteriae*, *C. albicans*, *Candida virusei* and *Candida virusei* (168). Moreover, stigmasterol from *S. spirale* had an MIC value of 1000 and 500 µg/mL against *E. coli* and *S. aureus*, respectively (114).

The anticancer activity of stigmasterol has been investigated and published. Stigmasterol showed strong cytotoxicity against Raji (lymphoma) and SK-MEL-28 (malignant melanoma cells) cancer cell lines with the IC₅₀ values of 0.17 and 3.90 µg/mL, respectively (166). In an *in vivo* study, stigmasterol showed significant therapeutic efficacy and protective effects against Ehrlich Ascites Carcinoma in mice (167). Female patients with ovarian cancers who consumed stigmasterol > 23 mg per day, found the risk of the ovarian cancer development was decreased (169). In addition, stigmasterol exhibited a significant antioxidative effect in the oxidation of methyl linoleate (170).

These bioactivities of stigmasterol could support the anticancer and antioxidant activities of the hexane fraction of *G. pictum* [PP1H]. Although stigmasterol had an antimicrobial activity, the fraction [PP1H] did

not inhibit any microbes. It may suggest that the lower concentration of the tested fraction [PP1H] or the other components of [PP1H] inhibit or mask the antimicrobial activity of stigmaterol.

4.10.2. Isolation and purification of the EtOAc fraction of *G. pictum* [PP1EA]

The EtOAc fraction [PP1EA] from the leaves of *G. pictum* [PP1] showed anticancer activity against MCF-7 (breast cancer cell line) with an IC₅₀ value of 26.01 µg/mL (Table 4.4). Therefore, this fraction was selected for further purification.

The EtOAc fraction [PP1EA] (501.5 mg) was subjected to normal phase column chromatography, using a gradient of hexane and EtOAc (100:0 to 0:100) followed by EtOAc and MeOH (90:10 to 0:100) as eluent to afford 7 fractions (Scheme 3.11). Fractions [1EA-3] and [1EA-4] showed the same major compound. Therefore, they were selected for further purification.

4.10.2.1. Isolation and purification of [1EA-3] and [1EA-4]

The combined fractions [1EA-3] and [1EA-4] (83.7 mg) were subjected to normal phase column chromatography, an isocratic elution of EtOAc (100 mL) followed by MeOH (30 mL) to afford 7 fractions (Scheme 3.12). Fractions [1EA-3.3], [1EA-3.4] and [1EA-3.5] showed the same major compound. Therefore, they were selected for further purification using column chromatography.

4.10.2.2. Isolation and purification of [1EA-3.3], [1EA-3.4] and [1EA-3.5]

The combined fractions [1EA-3.3], [1EA-3.4] and [1EA-3.5] (65.6 mg) were subjected to normal phase column chromatography using a gradient of hexane and EtOAc (60:40 to 0:100) followed by EtOAc and MeOH (95:5 to 0:100) as eluent to afford 7 fractions (Scheme 3.13). Fraction [1EA-3.3.2] and [1EA-3.3.3] showed impure crystals. Therefore, they were recrystallized from CHCl₃ to afford yellow crystalline needles,

6.0 and 1.8 mg, respectively. They were further identified using NMR spectroscopy and infrared spectroscopy. The ^1H NMR (500 MHz) spectrum of compound [1EA-3.3.3] (Appendix A Figure 5 page 268) indicated the presence of aromatic proton signals at δ 8.11, assigned to aryl protons at position-2, 3, 5 and 6, respectively. The methylene proton resonance appeared as singlet at δ 4.69. The carbonyl carbon was shown by the signal at δ 165.4 in the ^{13}C -NMR spectrum (Appendix A Figure 6, page 268). Aromatic ring carbon showed signals at δ 129.9 and 133.9. The HMBC correlations (Appendix A Figure 7, page 269) of this structure are shown in Figure 4.16. Moreover, the IR spectrum showed bands for the hydroxyl ($2969\text{-}2911\text{ cm}^{-1}$), carbonyl (1716 cm^{-1}) and aromatic ($1580\text{-}1408\text{ cm}^{-1}$) groups.

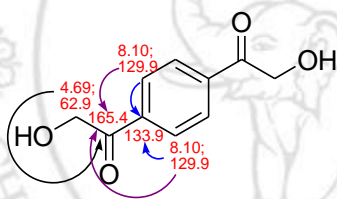


Figure 4.16 HMBC correlations for compound [1EA-3.3.3]

From these data, the structure of compound [1EA-3.3.3] was identified as 1,4-diglycoloyl-benzene (Figure 4.17) by the above evidences. The NMR spectroscopic data of compound [1EA-3.3.3] is shown in Table 4.22.

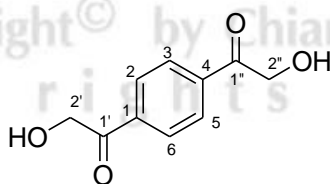


Figure 4.17 Chemical structure of [1EA-3.3.3]

Table 4.22 The NMR spectroscopic data of compound [1EA-3.3.3]

Position	δ_{exp} (500 MHz, CDCl ₃)	
	¹ H (mult, <i>J</i> (Hz))	¹³ C
1	-	133.9
2	8.10 (s, 1H)	129.9
3	8.10 (s, 1H)	129.9
4	-	133.9
5	8.10 (s, 1H)	129.9
6	8.10 (s, 1H)	129.9
1'	-	165.4
2'	4.69 (s, 2H)	62.9
1''	-	165.4
2''	4.69 (s, 2H)	62.9

1,4-Diglycoloyl-benzene has not been reported as a natural product. Chemical structure searching in SciFinder® database found this structure in the organic synthesis literature (171).

4.11. Isolation and purification of the crude extract of *S. spirale* [P2]

The previous study of Keawsa-ard (114) showed that the CHCl₃ extract of the stems of *S. spirale* had moderate anti-herpes simplex virus type-1 (HSV-1) activity. Therefore, the crude CHCl₃ extract [P2C] was selected for further isolation and purification.

4.11.1. Isolation and purification of the crude CHCl₃ extract of *S. spirale* [P2C]

The crude CHCl₃ extract of *S. spirale* [P2C] (1.7 g) was subjected to normal phase column chromatography, using a gradient of hexane and EtOAc (100:0 to 0:100) followed by EtOAc and MeOH (90:10 to 0:100) as eluent to afford 15 fractions (Scheme 3.15). The TLC of fraction [2C10] (162.8 mg) observed a blue spot under ultraviolet light at 365 nm. Therefore, it was selected for further purification.

4.11.1.1. Isolation and purification of [2C10]

The fraction [2C10] (161.4 mg) was subjected to normal phase column chromatography, using a gradient of hexane and EtOAc (60:40 to 0:100) followed by EtOAc and MeOH (90:10 to 0:100) as eluent to afford 8 fractions (Scheme 3.19). Fractions [2C10.6] and [2C10.7] showed the same major compound. Therefore, they were combined for further purification.

4.11.1.1.1. Isolation and purification of [2C10.6] and [2C10.7]

The combined fractions [2C10.6] and [2C10.7] (106.9 mg) were subjected to normal phase column chromatography over silica gel, using an isocratic elution of hexane:EtOAc (40:60) to afford 4 fractions.

Fractions [2C10.6.2] and [2C10.6.3] showed the same major compound which were separately purified using preparative TLC using hexane:EtOAc 2:3 as the eluent. Fraction [2C10.6.2] was separated in 2 fractions ([6.2.1] and [6.2.2]). Fraction [6.2.1] was further purified using preparative TLC using the same eluent to obtain 3 fractions ([6.2.1A], [6.2.1B] and [6.2.1C]) (Scheme 3.20), while [2C10.6.3] was separated in 3 fractions ([6.3.1], [6.3.2] and [6.3.3]) (Scheme 3.21).

Fractions [6.2.1C] (4.5 mg) and [6.3.2] (6.2mg) were found as crystals and showed a blue intense fluorescence at UV 365 nm which is characteristic of a coumarin. These compounds were further identified by NMR spectroscopy. They showed the same ^1H NMR data. The ^1H NMR (500 MHz) spectrum of compound [6.3.2] (Appendix A Figure 8 page 269) exhibited signals for two olefinic methine protons at δ 7.59 (d, $J = 9.5$ Hz, 1H, H-4), and 6.27 (d, $J = 10.0$ Hz, 1H, H-3). The two singlet aromatic proton resonances at δ 6.92 and 6.84 were assigned to H-8 and H-5. A methoxy group signal was observed at δ 3.95. Ten carbon signals were shown in the ^{13}C -

NMR spectrum (Appendix A Figure 9, page 270). The linkage position of the $-OCH_3$ was established by an HMBC experiment which showed the correlation between the proton signal at δ 3.95 (s, 3H) to C-6 at δ 144.5. The HMBC correlations of compound [6.3.2] are shown in Figure 4.18 (Appendix A Figure 10, page 270).

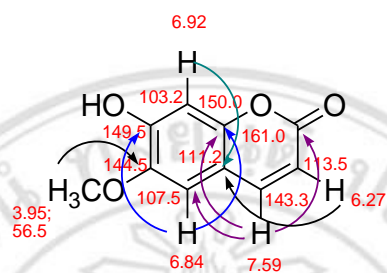


Figure 4.18 HMBC correlation of compound [6.3.2]

From these data, the structure of compound [1H-9.6] was identified as scopoletin (Figure 4.19) by the above evidences and from comparisons with previously published spectroscopic data (172-173) (Table 4.23).

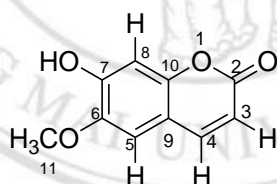


Figure 4.19 Chemical structure of scopoletin

ลิขสิทธิ์มหาวิทยาลัยเชียงใหม่
Copyright© by Chiang Mai University
All rights reserved

Table 4.23 Comparison of the NMR spectroscopic data of compound [6.3.2]

Position	δ_{exp} (500 MHz, CDCl ₃)		δ_{lit} (500 MHz (¹ H); 400MHz (¹³ C), CDCl ₃)	
	¹ H (mult, <i>J</i> (Hz))	¹³ C	¹ H (mult, <i>J</i> (Hz)) ^d (172)	¹³ C (173)
1	-	-	-	-
2	-	161.0	-	160.5
3	6.27 (d, <i>J</i> = 10.0, 1H)	113.5	6.30 (d, <i>J</i> = 9.5, 1H)	112.5
4	7.59 (d, <i>J</i> = 9.5, 1H)	143.3	7.68 (d, <i>J</i> = 9.5, 1H)	142.0
5	6.84 (s, 1H)	107.5	6.85 (s, 1H)	107.5
6	-	144.5	-	143.0
7	-	149.5	-	149.5
8	6.92 (s, 1H)	103.2	6.90 (s, 1H)	102.0
9	-	150.0	-	150.0
10	-	111.2	-	110.5
11	3.95 (s, 3H)	56.5	3.95 (s, 3H)	55.2

Compound [6.2.1C] was tested for antibacterial activity using the disc diffusion assay against *S. aureus* (ATCC 25923) and *E. coli* (ATCC 25922). Norfloxacin was used as the positive control and EtOH was used as the negative control. The results are shown in Table 4.24.

Table 4.24 Antibacterial activity of [6.2.1C]

Concentration of sample	Diameter of inhibition zone (mm) ^a	
	<i>S. aureus</i>	<i>E. coli</i>
[6.2.1C] 2.4 mg/mL	-	-
Norfloxacin (5µg/disc)	28.0	32.0
Ethanol	-	-

^aInhibition zones are the mean diameter of disc 5 mm

Compound [6.2.1C] at the concentration of 2.4 mg/mL had no antibacterial activity against both *S. aureus* and *E. coli*.

Scopoletin is a 6-methoxy-7-hydroxycoumarin which is a member of the phenolic coumarins. It was isolated from many plant

species such as *Ipomoea batatas* and *Solanum lyratum*. Plants containing scopoletin or only scopoletin have been used as traditional medicines in Africa, Europe and Asia for the treatment of various symptoms, for examples; convulsion, inflammation and rheumatic pain (174).

Many publications revealed that scopoletin was able to inhibit various bacteria and fungi strains (175-177). Although scopoletin revealed an antimicrobial activity, our study showed no activity against the tested bacteria.

Moreover, the biological activities of scopoletin have been revealed. Scopoletin had cytotoxic activities against P-388 murine leukemia and MDA-MB-human adenocarcinoma mammary grand cells with IC₅₀ values of 17.42 and 10 µg/mL, respectively (178-179). In addition, scopoletin showed the ability to induce apoptosis in HL-60 cell (human leukemia cell line) by the activation of nuclear factor-kappa B (NF-κB) and the activation of caspase-3 (180).

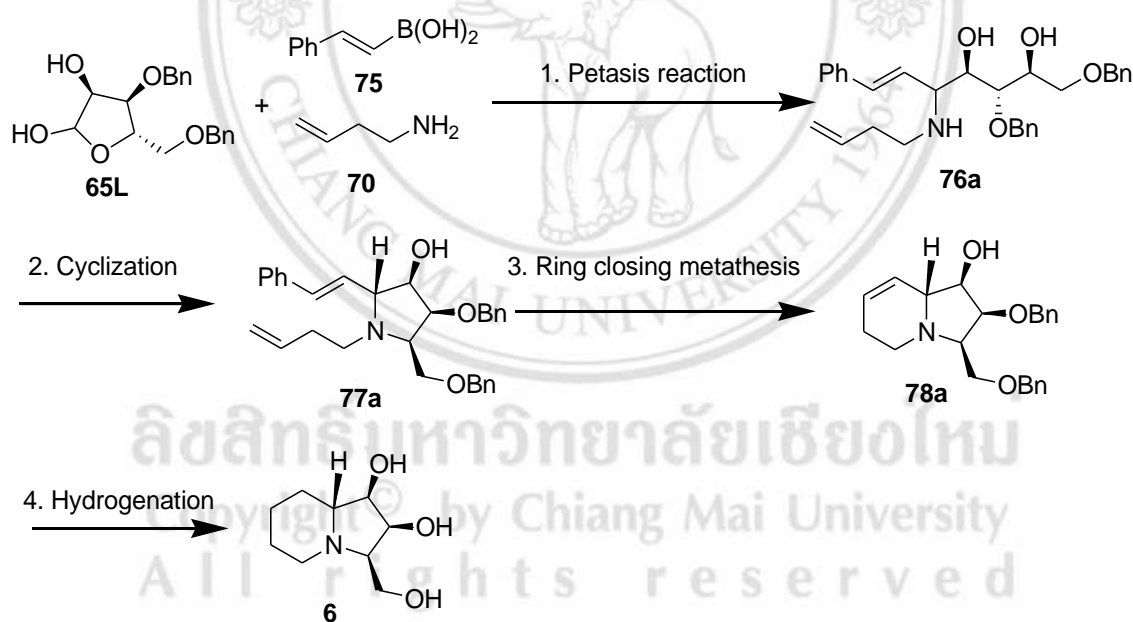
Scopoletin also showed significant antioxidant activities using *in vitro* antioxidant assays; DPPH[•], ABTS^{•+}, hydrogen peroxide, superoxide, hydroxyl radical scavenging activities, ferrous ion chelating activity and β-carotene bleaching assay (181-183).

The anti-inflammation effect of scopoletin has been reported. Yao *et al.* (184) showed that scopoletin could inhibit monosodium urate crystal-induced inflammation *in vivo* and *in vitro* studies. Scopoletin also inhibited the 5-lipoxygenase enzyme which is involved in chronic inflammatory and allergy diseases (183). Moreover, scopoletin could inhibit the acetylcholinesterase enzyme (183). The *in vitro* study showed that scopoletin had a hepatoprotective activity (185). According to these interesting activities, scopoletin or plant containing scopoletin should be selected for further drug discovery.

CHAPTER 4

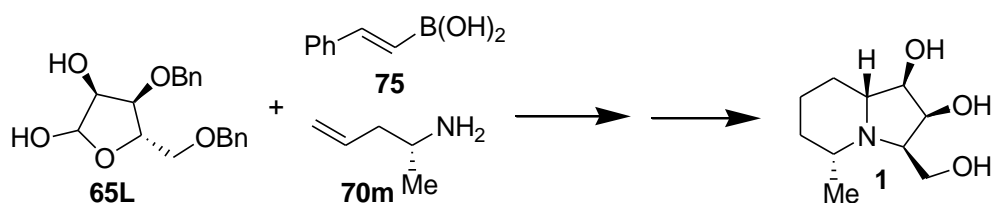
Results and discussion

As well as the synthesis of natural (-)-steviamine [1] and 5-*epi-ent*-steviamine [7], we also planned to synthesize the relative simple 10-*nor*-analogue of (-)-steviamine [6]. Several key reactions would be tested (Scheme 4.1). In particular, we observed whether the Petasis reaction would facilitate a stereoselective entry into the *anti*-1,2 amino alcohol [76a] and whether this molecule would undergo cyclization, to give the fully substituted pyrrolidine [77a]. Then, compound 77a would undergo a ring closing metathesis (RCM) reaction to form the corresponding indolizidine [78a]. If successful, hydrogenation of 78a would be followed by the removal of protecting groups to give the final target product [6].



Scheme 4.1. Synthetic plan for the 10-*nor*-analogue of (-)-steviamine [6].

If the syntheses were successful then (-)-steviamine [1] could be synthesized following these synthetic protocols by changing only 3-buten-1-amine [70] to (*R*)-pent-4-*en*-2-amine [70m] (Scheme 4.2).

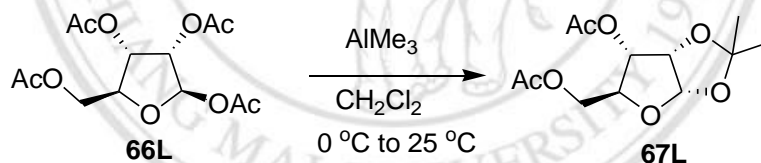


Scheme 4.2. Synthetic plan for (-)-steviamine [1].

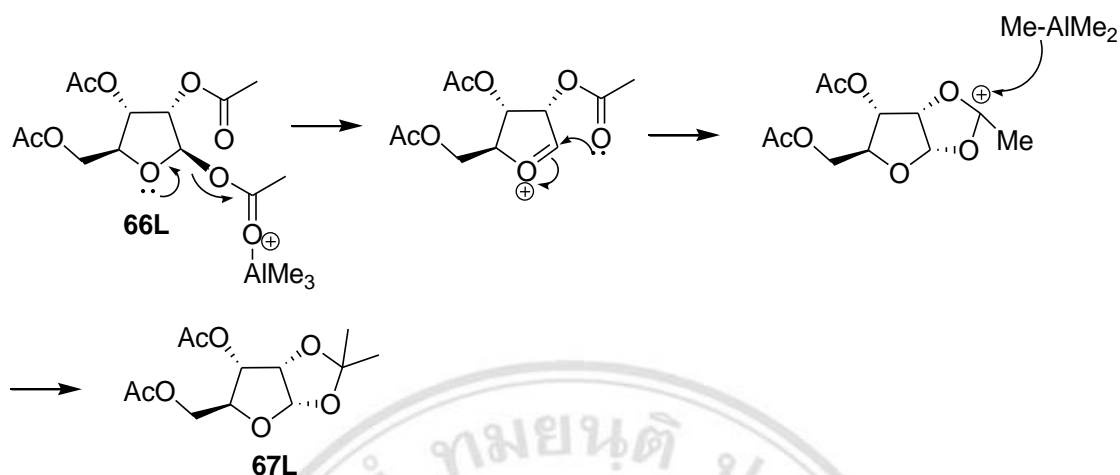
Originally, the β -L-ribofuranose 1,2,3,5-tetraacetate derivative [65L], 3-buten-1-amine [70] and *trans*-2-phenylvinylboronic acid [75] were the planned as the starting materials for the Petasis reaction in Scheme 4.2. The β -L-ribofuranose 1,2,3,5-tetraacetate derivative [65L] was firstly prepared from commercially available β -L-ribofuranose 1,2,3,5-tetraacetate [66L].

4.1 The synthesis of β -L-ribofuranose 1,2,3,5-tetraacetate derivative ((3*S*,4*R*,5*S*)-4-(benzyloxy)-5-(benzyloxymethyl)tetrahydrofuran-2,3-diol) [65L]

4.1.1 The synthesis of the 1,2-isopropylidene acetal of per-acetylated ribofuranose

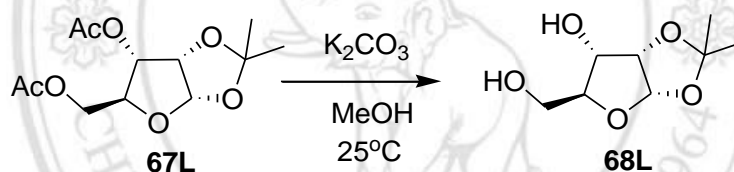


The synthetic procedure of More and Campbell (1) was followed. Commercially available β -L-ribofuranose 1,2,3,5-tetraacetate [66L] (1 equivalent) was used as a starting material which was treated with 2 equivalents of trimethylaluminium (AlMe_3) in CH_2Cl_2 at $0\text{ }^\circ\text{C}$ followed by slowly warming to rt ($25\text{ }^\circ\text{C}$) and stirring for 15 h. After quenching and purification by column chromatography, the 3,5-*O*-acetyl-1,2-*O*-isopropylidene ribofuranose anoside [67L] was obtained in 79% yield as a clear viscous oil which was used as a starting material in the next step. The $^1\text{H-NMR}$ spectrum of **67L** matched with that reported in the literature (242). The mechanism of this reaction is shown in Scheme 4.3.



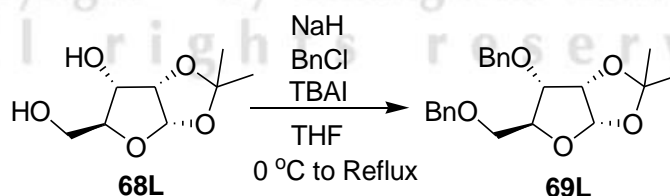
Scheme 4.3. The mechanism of the synthesis of the 1,2-isopropylidene acetal of per-acetylated ribofuranose.

4.1.2 Deacetylation



Using the procedure of Kim *et al.* (244), compound **67L** (1 equivalent) was subjected to deacetylation using K_2CO_3 (3 equivalents) in MeOH at rt for 2 h. After quenching and filtration, the diol [**68L**] was afforded in 85% yield as a white solid which was used without further purification. The 1H -NMR spectrum of **68L** matched with that reported in the literature (245).

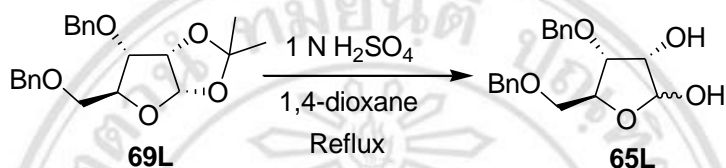
4.1.3 O-Benzoylation



Protection of the two hydroxyl groups of **68L** was achieved using a slightly modified procedure of Matsuda *et al.* (246). A solution of compound **68L** in anhydrous THF was slowly added to a suspension of sodium hydride (NaH) in anhydrous THF at 0 °C. The reaction mixture was then heated under reflux for 5 min. After re-cooling to rt,

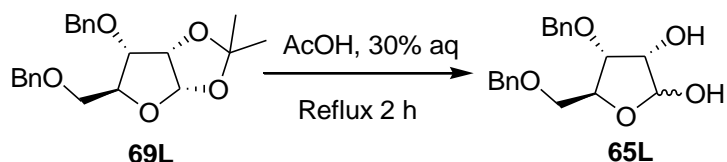
benzyl chloride (BnCl) and tetrabutylammonium iodide (TBAI) were added to the reaction mixture which was then heated under reflux for further 30 min until TLC control showed full consumption of the starting material. After quenching and purification with a column chromatography, the desired product [**69L**] was obtained in 72% yield as a pale yellow viscous oil which was used for the last step. The $^1\text{H-NMR}$ spectrum of **69L** matched with that reported in the literature (259).

4.1.4 Isopropylidene hydrolysis



In the last step, the hydrolysis of the acetonide group of **69L** was performed according to the method of Lafont *et al.* (248) using H_2SO_4 in 1,4-dioxane. The reaction mixture was heated under reflux at $100\text{ }^\circ\text{C}$ and stirred for 3 hrs. The reaction was checked by TLC every hour. After work up of the reaction mixture, the crude product was purified by flash column chromatography to afford the desired compound [**65L**] (9%) as a white solid.

This method produced a lot of side products and gave the final product [**65L**] in very low yield. This problem might be due to in the inappropriate reflux temperature control which may let the temperature increased higher than $100\text{ }^\circ\text{C}$. This condition might effect on the desired product [**65L**] which the product may be changed to other compounds. From this result, another method was found. Lucas *et al.* (249) reported a method to hydrolyze an isopropylidene using 30% aqueous acetic acid and reflux. The reaction is shown below:



Compound [**69L**] was dissolved in 30% aqueous acetic acid (AcOH) and refluxed ($\sim 112\text{ }^\circ\text{C}$) for 2 h. The reaction mixture was then cooled in an ice bath over 1 h and the product began to precipitate. The reaction mixture was diluted with CH_2Cl_2 then

quenched with sat. NaHCO₃. The CH₂Cl₂ solution was dried over MgSO₄, filtered and concentrated *in vacuo* to obtain the final product [65L] as a white solid (94%). This method was not complicated and provided a desired product in a high yield without purification. The ¹H-NMR spectrum of 65L showed a mixture of anomers, and matched with that reported in the literature (250). The next step is to synthesize 10-*nor*-steviamine [6].

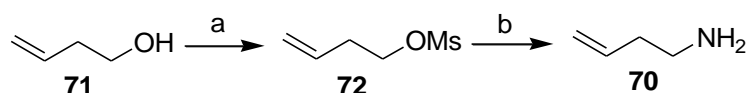
4.2 The synthesis of 10-*nor*-steviamine [6]

The synthesis of 10-*nor*-steviamine [6] (Scheme 4.2) was planned in four steps which consisted of the Petasis reaction, cyclization, ring closing metathesis (RCM) and hydrogenation.

4.2.1 The Petasis reaction

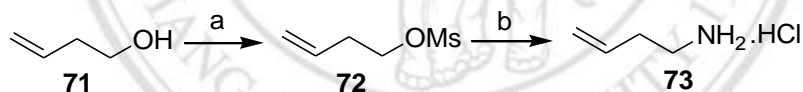
The Petasis reaction (or boronic acid Mannich reaction) is very useful reaction for the preparation of the chiral *anti*-1,2-amino alcohol moieties. These have been used as building blocks for the synthesis of polyhydroxylated pyrrolizidines and indolizidines, including the proposed structure of uniflorine A, casuarine, australine, 3-*epi*-australine, hyacinthacine B₃, the proposed structure of hyacinthacine B7. The Petasis reactions are multicomponent reactions which consist of the three components; boronic acids (aryl, alkenyl, alkynyl, allyl and including their esters or related potassium trifluoroborates), carbonyl compounds (aldehydes and ketones which are usually α -hydroxy substituted ones or glyoxylic acids), and amino compounds (ammonia, primary and secondary amines, mono-*N*-protected hydrazines, hydroxylamines, methoxyamines, and sulfinamides) (260-261).

For the Petasis reaction, the β -L-ribofuranose 1,2,3,5-tetraacetate derivative [65L], 3-butenylamine [70] and *trans*-2-phenylvinylboronic acid [75] were used as starting materials. The 3-butenylamine [70] was synthesized using the modified method of Yazici and Pyne (251) as follows:



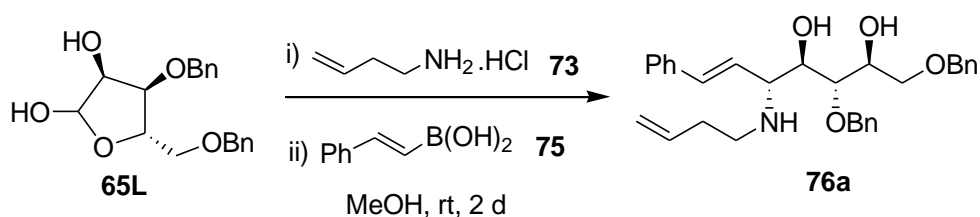
Scheme 4.4. *Reagents and conditions:* (a) MsCl, Et₃N, CH₂Cl₂, 0 °C to rt; (b) 28% NH₃ (aq), MeOH, rt, 2 d.

Commercially available 3-buten-1-ol [71] (1 equivalent) and Et₃N (1.5 equivalents) were dissolved in dry CH₂Cl₂. To this mixture was then added dropwise MsCl (1.5 equivalents) at 0 °C. The resulting mixture was stirred at rt for 18 h. After a standard work up procedure, the *O*-mesylate product [72] was obtained as yellow liquid. In the next step, compound [72] was dissolved in MeOH and then aqueous ammonia solution was added. After the reaction mixture was stirred at rt for 2 days, the solution was diluted with water and extracted with CH₂Cl₂. The combined organic extracts were dried over MgSO₄, filtered and carefully concentrated to give an amine [70] (10%) as a yellow liquid. All of the CH₂Cl₂ was purposely not remove from this amine because of its volatility. The better way to isolate this amine was a modification of this amine [70] to its less volatile HCl salt form [73].



Scheme 4.5. *Reagents and conditions:* (a) MsCl, Et₃N, CH₂Cl₂, 0 °C to rt; (b) 28% NH₃ (aq), MeOH, rt, 2 d.

The HCl salt form of amine [73] was prepared using the same procedures of the synthesis of compound 70, but it differed slightly in the last work-up step. The reaction mixture from step b (Scheme 4.5) was diluted with water and extracted with Et₂O. The combined organic extracts were dried over MgSO₄ and filtered. Then 2 M HCl in Et₂O was then added. The aqueous phase was separated and concentrated *in vacuo* to obtain the final product [73] as a white solid (18% over two steps). As a result, this synthesis gave a quite low percentage yield, so commercially available 3-butenylamine·hydrochloride (Aldrich) was selected to use for this Petasis reaction.



Scheme 4.6. The Petasis reaction of compound **65L**.

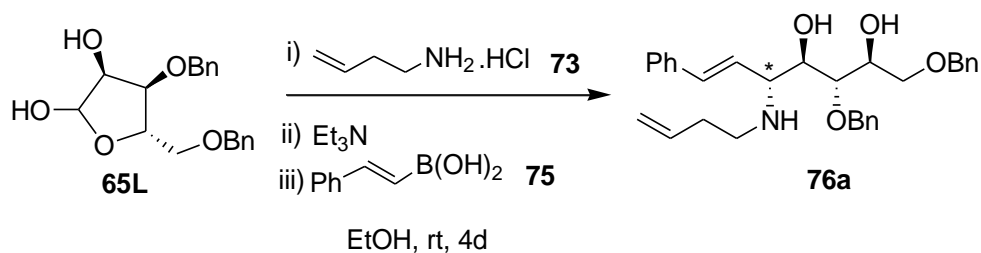
The reaction between the β -L-ribofuranose 1,2,3,5-tetraacetate derivative [**65L**], 3-butenylamine·hydrochloride [**73**] and *trans*-2-phenylvinylboronic acid [**75**] was carried out as shown in Scheme 4.5 which was modified from a method of Moosophon *et al.* (252). This reaction was monitored using a TLC control and checked by a low-resolution mass spectrometry every day. However, we could not detect the desired product [**76a**]. It is possible that 3-butenylamine·hydrochloride is not active, so we decided to add triethylamine (Et_3N) which will help to generate a free amine of 3-butenylamine·hydrochloride [**73**]. The reaction mixture was then stirred for 18 h. TLC control showed the product. Finally, the amino diol [**76a**] was obtained, as a single diastereomer in 10% yield, after purification by column chromatography. Moreover, the study of several different solvents on the yield of this reaction was compared and the results are shown in Table 4.1.

Table 4.1. Optimization of the Petasis reaction of compound **76a**^a

Entry	Solvents	Time (days)	Yield (%)
1	Acetonitrile	3	0
2	EtOH	4	59
3	CH ₂ Cl ₂ + HFIP ^{b,c}	2	30
4	CH ₂ Cl ₂	2	20
5	EtOH + HFIP ^{b,c}	3	13

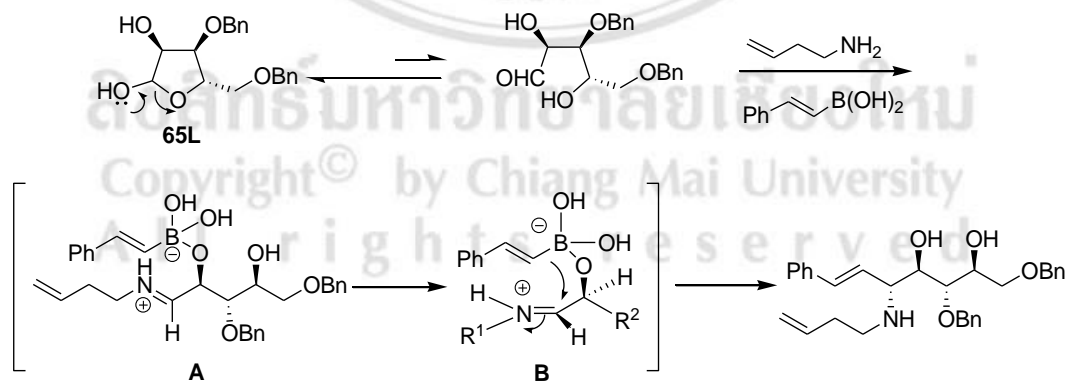
^aReactions were performed with the β -L-ribofuranose 1,2,3,5-tetraacetate derivative [**65L**] (1 equivalent), 3-butenylamine-hydrochloride [**73**] (1 equivalent), *trans*-2-phenylvinylboronic acid [**75**] (1 equivalent) and Et₃N (1 equivalent), ^bHFIP = 1,1,1,3,3,3-hexafluoro-2-propanol, ^cused 10% of each solvent volume.

From Table 4.1, acetonitrile was not effective at room temperature which showed no synthetic product. The combination of CH₂Cl₂ with HFIP performed better than only CH₂Cl₂. In contrast, the combination of EtOH with HFIP gave a lower yield than only EtOH. The use of EtOH was the most effective among the tested solvents. Therefore, the best Petasis reaction synthesized an amino diol [**76a**] was concluded in Scheme 4.7. The configuration at the newly created, amino group bearing, stereogenic center (*) in **76a**, indicated a single diastereomer had formed and would become C8a in the final target [**6**]. The ¹H-NMR spectrum of **76a** showed resonances for five olefinic protons (δ 6.51, 6.23, 5.77-5.67, 5.07 and 5.03), and two *O*-benzyl groups (δ 4.64, 4.56, 4.55 and 4.47), as well as resonances for the other aromatic methine and methylene groups (see Chapter 3). The ¹³C NMR spectrum was also consistent with the structure of **76a** (see Chapter 3) as well as its HRMS ((M+H)⁺, *m/z* 488.2784).



Scheme 4.7. The best conditions for the Petasis reaction of compound **65L**.

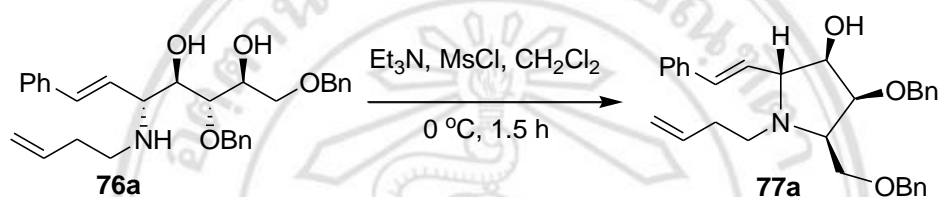
The exact mechanism of the Petasis reaction is unknown. The proposed reaction mechanism (Scheme 4.8) starts with a ring-opening of the β -L-ribofuranose 1,2,3,5-tetraacetate derivative [**65L**] to give the aldehyde form, which reacts with 3-buten-1-amine to form an iminium ion. The *trans*-2-phenylvinylboronic acid then coordinates to the hydroxyl group of the iminium ion at the C-2 position to give the boronate intermediate **A**. This complex adopts the reactive conformation **B** to minimize 1,3-allylic strain between the allylic α -substituent and the NH of the iminium ion. Intramolecular transfer of the styryl group on the β -face of the iminium ion provides the desired *anti*-amino diol (260,262). The other hydroxyl groups of the iminium ion can also coordinate with boron to form a complex but this process is a reversible reaction. These boronate intermediates are less likely to lead to product because of their more remote distance of the styryl group to the iminium ion.



Scheme 4.8. Proposed reaction mechanism of the Petasis reaction.

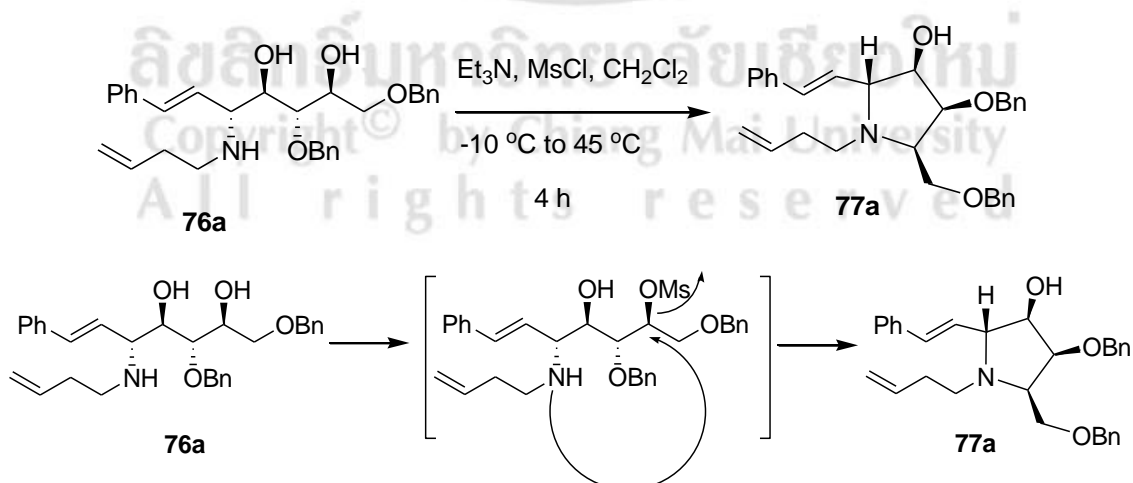
4.2.2 O-mesylation cyclization

In this step, the primary alcohol of **76a** was converted into a good leaving group using mesyl chloride before cyclization. The procedure of Au *et al.* (253) was used and slightly modified. Alcohol [**76a**] (1 equivalent) was dissolved in CH₂Cl₂ at 0 °C. To this solution was then added triethylamine (1 equivalent) and a 0.13 M solution of methanesulfonyl chloride in CH₂Cl₂ (1.2 equivalents). The reaction mixture was stirred at 0 °C for 1.5 h (Scheme 4.9).



Scheme 4.9. The mesylation–cyclization reaction of compound **76a**.

After a basic work up the crude product was purified by flash column chromatography to afford the desired compound [**77a**] (40%) as a yellow oil. This reaction gave quite a low yield and resulted in other side products. Therefore, we changed the synthetic condition followed Bouillon and Pyne (254) This second mesylation cyclization of compound **76a** still used the same reagents but the reaction temperature and time conditions were changed (Scheme 4.10).



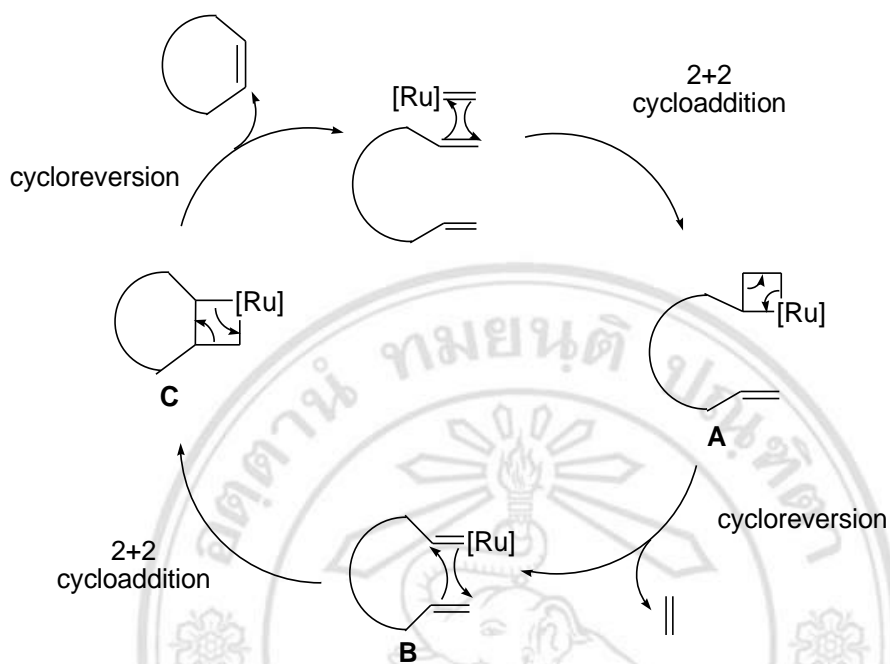
Scheme 4.10. The second mesylation cyclization of compound **76a**.

Treatment of compound **76a** with 1.07 equivalents of methanesulfonyl chloride and 3.5 equivalents of triethylamine, followed by warming of the *O*-mesylate intermediate to 45 °C for 4 h provided the fully substituted pyrrolidine [**77a**] in 83% yield after separation of small amounts of *O,N*-dimesylated **76a** and unreacted **76a** by column chromatography. This reaction is a result of the selective mesylation of the least hindered side chain hydroxyl group of **76a** followed by cyclization by nucleophilic attack by the N atom as shown in Scheme 4.8. The ¹H-NMR spectrum of **77a** showed resonances for five olefinic protons (δ 6.56, 6.03, 5.79-5.72, 4.99 and 4.95), and two *O*-benzyl groups (δ 4.76, 4.51, 4.60 and 4.57), as well as resonances for the other aromatic methine and methylene groups (see Chapter 3). The NOESY NMR experiment also indicated the correlation between H-2 and H-8 and H-2 and H-3. The ¹³C NMR spectrum corresponded with the structure of **77a** (see Chapter 3) as well as its HRMS ((M+H)⁺, m/z 470.2674).

4.2.3 Ring closing metathesis (RCM)

The RCM reaction is the third step of our synthetic plan to prepare the indolizidine ring. The proposed mechanism of RCM is shown in Scheme 4.11. The least hindered alkene of the diene coordinates to the ruthenium catalyst [Ru] to form an intermediate ruthenium complex **A** which upon a cycloreversion reaction loses ethene and gives the ruthenium carbene intermediate **B**. A second [2+2] cycloaddition produces an intermediate metallacyclobutane **C** which undergoes a cycloreversion to give the product and regenerates the catalyst (263).

ลิขสิทธิ์ © โดย Chiang Mai University
All rights reserved



Scheme 4.11. The proposed mechanism of the RCM reaction.

Following the same method of Au *et al.* (255), the RCM of our pyrrolidine compound **[77a]** used 18 mol% Grubbs' second generation catalyst (Figure 4.1) with heating at reflux for 2.5 h in CH_2Cl_2 , in the presence of 0.2 equivalents of titanium tetrakisopropoxide ($\text{Ti}(\text{O}^i\text{-Pr})_4$) (Scheme 4.12).

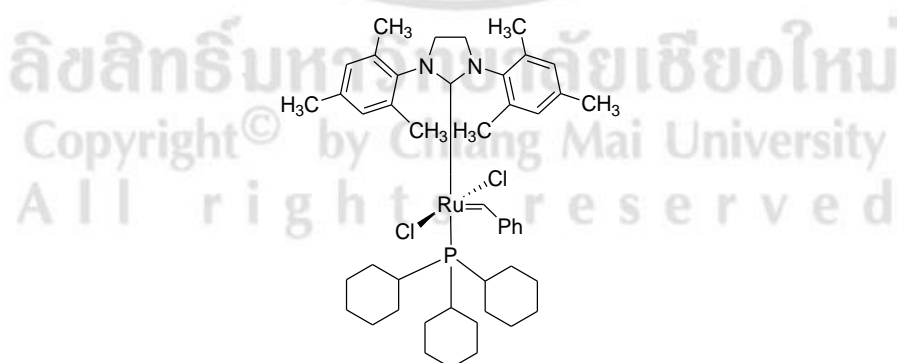
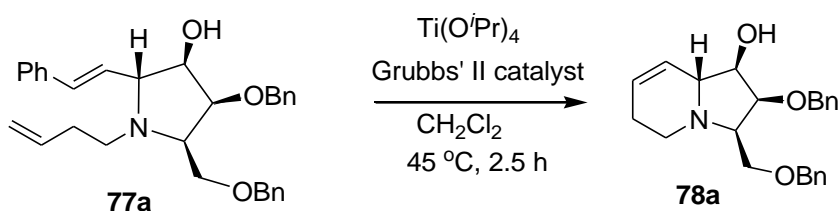


Figure 4.1. Structure of Grubbs' second generation catalyst.

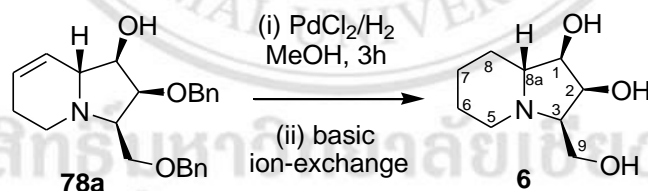


Scheme 4.12. The RCM reaction of pyrrolidine **77a**.

Ti(O^{*i*}-Pr)₄ is a Lewis acid which was used for deactivation of the amino group of **77a** by preventing the N-atom from coordinating to the ruthenium metal center (264). The indolizidine [**78a**] was obtained in 62% yield after purification by column chromatography (Scheme 4.12). ¹H-NMR analysis of **78a** confirmed that the successful synthesis of the indolizidine ring had occurred, by a reduction of the five alkene resonances to two alkene resonances (δ 5.84-5.82 and 5.62) and disappearance of the five aromatic methines of **77a** (see Chapter 3).

4.2.4 Hydrogenation

Hydrogenation and hydrogenolysis of the indolizidine [**78a**] followed the procedure of Ritthiwigrom *et al.* (256) using PdCl₂/H₂ gave 10-*nor*-steviamine [**6**] in 100% yield after neutralization of the HCl salt of **6** and purification by basic ion-exchange chromatography (Scheme 4.13).



Scheme 4.13. The hydrogenation of indolizidine **78a**.

10-*Nor*-steviamine [**6**] was first synthesized in 2012 by Gómez *et al.* (194) using a chemoenzymatic synthesis of novel indolizidine iminocyclitols. The physical properties and the NMR spectral data between the literature and the synthetic 10-*nor*-steviamine [**6**] are compared and summarized in Table 4.2.

Table 4.2. Physical and the NMR spectral data of literature (194) and synthetic 10-*nor*-steviamine [6].

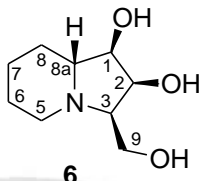
	Literature (194)	Synthetic [6]
Structure	 6	
Physical Appearance	-	Brown oil
Optical Rotation	$[\alpha]_D^{22} -8.7$ (c 1.2, H ₂ O)	$[\alpha]_D^{25} -7.7$ (c 1.0, H ₂ O) $[\alpha]_D^{25} -11.4$ (c 0.6, MeOH)
¹ H-NMR	600 MHz, D ₂ O	500 MHz, D ₂ O (Appendix B Figure 7, page 274)
	4.39 (t, ³ J(H,H) = 6.4 Hz, 1H)	4.40 (t, J = 6.5 Hz, 1H, H-2)
	3.87 (t, ³ J(H,H) = 5.7 Hz, 1H)	3.87 (dd, J = 12.0, 5.5 Hz, 1H, H-9)
	3.83 (dd, ³ J(H,H) = 12.2, 5.0 Hz, 1H)	3.82 (t, J = 6.0 Hz, 1H, H-1)
	3.77 (dd, ³ J(H,H) = 12.2, 5.5 Hz, 1H)	3.81 (dd, J = 12.0, 5.0 Hz, 1H, H-9)
	3.41 (m, 1H)	3.30 (dd, J = 12.5, 5.5 Hz, 1H, H-3)
	3.02 (m, 1H)	2.96-2.93 (m, 1H, H-5)
	2.97 (s, 1H)	2.76-2.74 (m, 1H, H-8a)
	2.83 (t, ³ J(H,H) = 10.0 Hz, 1H)	2.72-2.67 (m, 1H, H-5)
	1.80 (m, 1H)	1.87-1.84 (m, 1H, H-8)
	1.70 (m, 1H)	1.80-1.76 (m, 1H, H-7)
	1.57 (m, 1H)	1.62-1.58 (m, 1H, H-6)

Table 4.2. (continued)

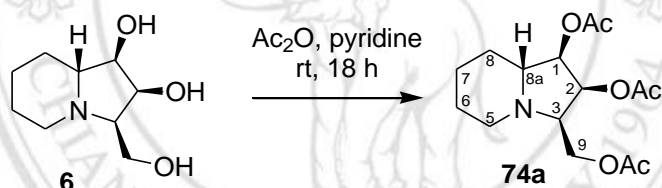
	Literature (194)	Synthetic [6]
¹ H-NMR	600 MHz, D ₂ O	500 MHz, D ₂ O (Appendix B Figure 7, page 274)
	1.50 (m, 2H)	1.54-1.46 (m, 1H, H-6)
	1.30 (m, 3H)	1.41-1.32 (m, 1H, H-7)
		1.29-1.21 (m, 1H, H-8)
¹³ C-NMR	151 MHz, D ₂ O	125 MHz, D ₂ O (Appendix B Figure 8, page 274)
	73.6	74.5 (C-1)
	69.7	70.1 (C-2)
	64.2	64.0 (C-3)
	63.7	63.8 (C-8a)
	57.8	58.5 (C-9)
	47.1	47.3 (C-5)
	25.3	27.2 (C-8)
	21.5	23.1 (C-6)
	21.3	22.7 (C-7)

From Table 4.2, our compound **6** had a specific rotation of $[\alpha]_{\text{D}}^{25} -7.7$ (*c* 1.0, H₂O) which was similar to that reported in the literature (194) $[\alpha]_{\text{D}}^{22} -8.7$ (*c* 1.2, H₂O), however, there were significant differences between these two compounds in the ¹H NMR spectral data recorded in D₂O.

The most significant difference was the relative chemical shifts for the protons H-1 and H-9a and H-9b in the range of $\delta \sim 3.8$ -3.9. In our sample the H-9 protons were observed as dd resonances (*J* = 12.0, 5.0-5.5 Hz) at δ 3.87 and δ 3.81 while the H-1 resonance at δ 3.82 (apparent t, *J* = 6.0 Hz) was observed at a chemical shift in between

those of the two H-9 resonances. The literature (194), however, reported the H-9 protons as dd resonances ($J = 12.2, 5.0\text{--}5.5$ Hz) at δ 3.83 and δ 3.77 with the H-1 signal being the most downfield of this group at δ 3.87 (apparent t, $J = 5.5$ Hz). Further, H-8a resonated at δ 2.67–2.72 (m) in our sample while the literature value for the chemical shift of this proton was δ 2.97 (s).

The ^{13}C NMR chemical shifts were also significantly different with the chemical shift differences varying from -1.9 to 0.2 ppm. Since NOESY (Appendix B, Figure 9, page 275) and ROESY (Appendix B, Figure 10, page 276) NMR experiments on our sample [6] were not unequivocal in defining the stereochemistry of our compound, because of the closeness of the individual resonances, and because the NMR chemical shifts of these types of polyhydroxylated compounds in D_2O can vary with pH and concentration (256,265), we therefore prepared **74a**, the triacetate derivative of 10-*nor*-steviamine [6] (Scheme 4.14).



Scheme 4.14. The acetylation of 10-*nor*-steviamine [6].

The compound **6** was acetylated with an acetic anhydride (Ac_2O) in dry pyridine using a slight modification of the procedure of Davis *et al.* (257) After purification by flash column chromatography, the triacetate derivative [**74a**] was obtained in 86% yield as a yellow oil.

The ROESY NMR experiments of this triacetate derivative [**74a**] in CDCl_3 (Appendix B Figure 13, page 278) clearly indicated the correctly assigned stereochemistry of **74a**. Significant cross peaks were observed between H-9 and H-5 β and H-8a and both H-5 β and H-9, which clearly supported the relative *syn*-stereochemical relationship between these three protons (Figure 4.2).

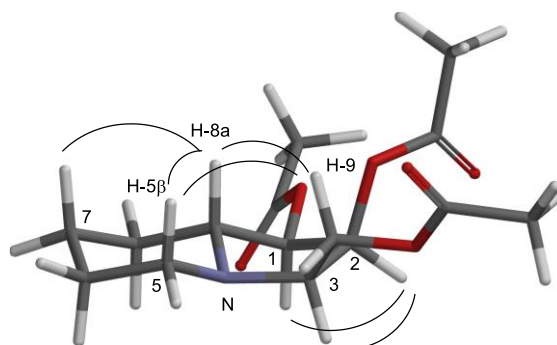
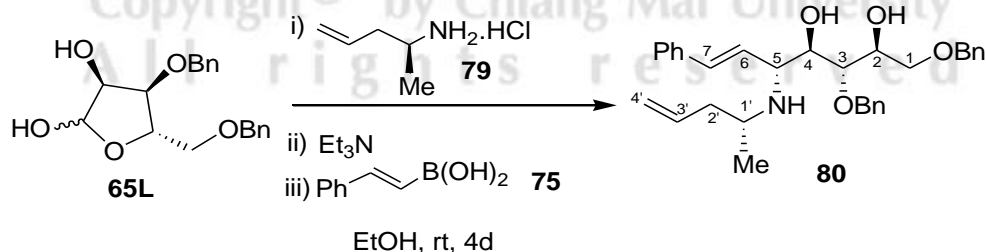


Figure 4.2. Significant ROESY cross-peaks of compound **74a** (SPARTAN generated structure using a DFT calculation (B3LYP/6-31G** level)).

These ROESY NMR correlations of the triacetate derivative [**74a**] confirmed that our proposed structure of 10-*nor*-steviamine [**6**] was correct. The total synthesis of 10-*nor*-steviamine [**6**] was thus achieved in eight synthetic steps from commercially available β -L-ribofuranose-1,2,3,5-tetra-*O*-acetate. This concise synthetic strategy was further employed to prepare (–)-steviamine [**1**].

4.3 The synthesis of (–)-steviamine [**1**].

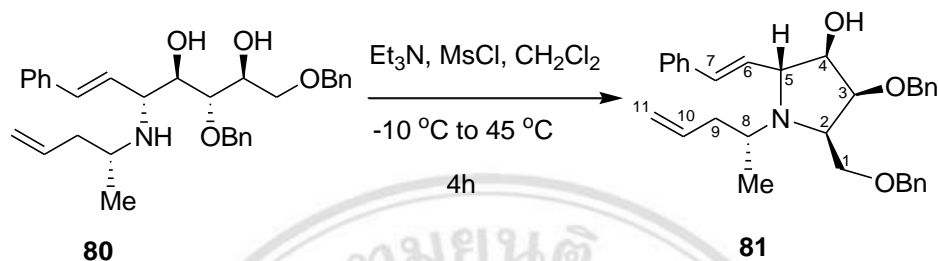
(–)-Steviamine [**1**] was prepared using the same procedures of the synthesis of 10-*nor*-steviamine [**6**]. The first step started with the Petasis reaction between the β -L-ribofuranose derivative [**65L**], commercially available (*R*)-4-penten-2-amine·HCl [**79**] (instead of 3-butenylamine·hydrochloride [**73**]), triethylamine and *trans*-2-phenylvinylboronic acid [**75**] (Scheme 4.15).



Scheme 4.15. The Petasis reaction in the synthesis of (–)-steviamine [**1**].

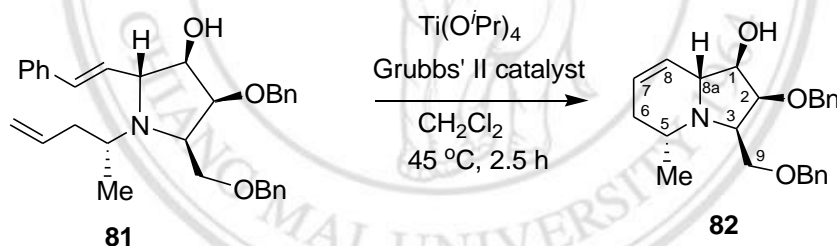
After purification of the crude reaction mixture by column chromatography, the amino alcohol [**80**] was obtained in 77% yield, as a single diastereomer. The ^1H and ^{13}C

NMR spectra of **80** were similar to those of **76a** except for the Me doublet resonance at δ 1.04 (d, $J = 6.5$ Hz) in the ^1H NMR spectrum of **80** and the extra carbon resonance for the Me group at δ 19.2.



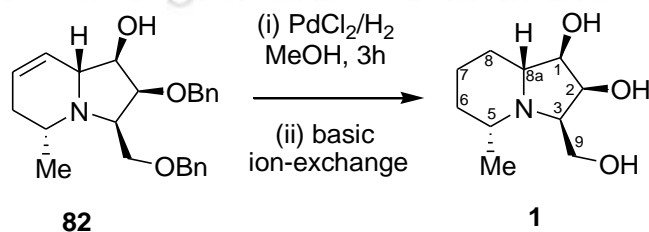
Scheme 4.16. The mesylation cyclization of compound **80**.

The second step, treatment of **80** with methanesulfonyl chloride and triethylamine followed by warming of the *O*-mesylate intermediate to 45 °C for 4 h provided the fully substituted pyrrolidine [**81**] in 66% yield after separation of small amounts of *O,N*-dimesylated **80** and unreacted **80** by column chromatography (Scheme 4.16).



Scheme 4.17. The RCM reaction of pyrrolidine **81**.

In the third step, a ring-closing metathesis reaction of diene [**81**] using 18 mol% Grubbs' second generation catalyst, in the presence of $\text{Ti}(\text{O}^i\text{-Pr})_4$ to deactivate the amino group in **81**, gave the indolizidine **82** in 76% yield (Scheme 4.17).



Scheme 4.18. The hydrogenation of indolizidine **82**.

In the last step, indolizidine **[82]** underwent hydrogenation/hydrogenolysis with PdCl₂/H₂ (Scheme 4.18). After neutralization/purification by basic ion-exchange chromatography, (–)-steviamine **[1]** was obtained in quantitative yield (100%) as a brown oil. The ¹H-NMR spectrum of **1** showed the disappearance of the alkene signals (δ 5.79-5.76 and 5.53) and loss of the ten aromatic proton resonances (δ 7.34-7.21) of **82**, while the ¹³C-NMR spectrum also showed the disappearance of two *O*-benzyl groups of **82** (two quaternary carbons (δ 138.4 and 137.5), ten aromatic carbons (δ 128.4, 128.3, 128.2, 127.8 and 127.6) and two methylene groups (δ 74.0 and 71.5)) and two alkene CH signals (δ 129.1 and 127.7) of **82** (see Chapter 3). The 1D-NOESY and ROESY could define the stereochemistry of our synthetic (–)-steviamine which showed significant cross peaks between H-9 and H-5_β, H-5_β and H-8a, H-8a and H-9, H-3 and H-2 and H-2 and H-1 as shown in Figure 4.3.

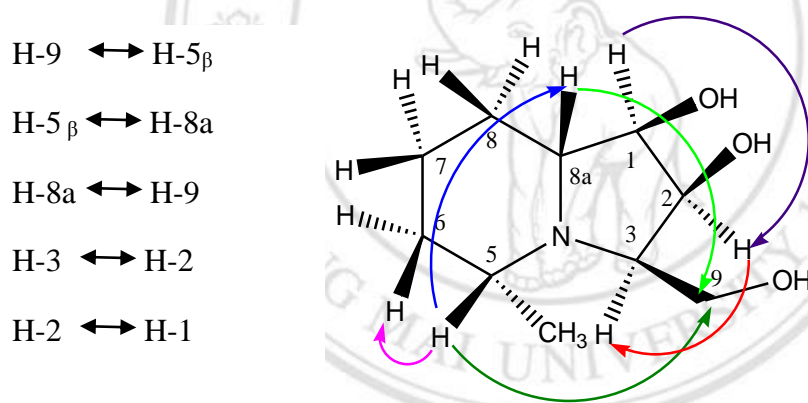


Figure 4.3 1D-NOESY and ROESY correlations of synthetic (–)-steviamine **[1]**.

The physical properties and the NMR spectral data between the natural (–)-steviamine which was reported by Michalik *et al.* (189) and the synthetic (–)-steviamine **[1]** are compared in Table 4.3.

Table 4.3. Physical and the NMR spectral data of natural (-)-steviamine (189) and synthetic (-)-steviamine [1].

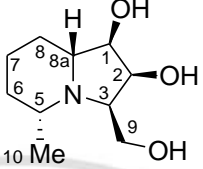
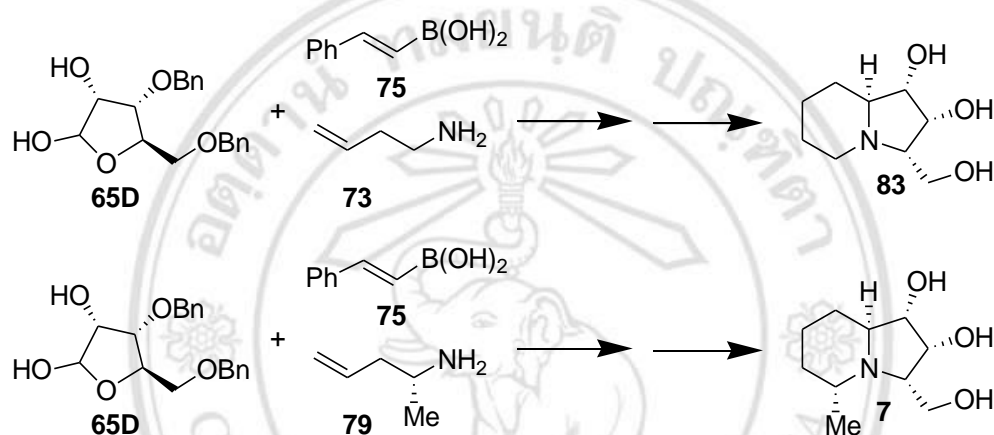
	Natural (-)-steviamine (189)	Synthetic [1]
Structure		
Physical Appearance	-	Brown oil
Optical Rotation	$[\alpha]_D^{20} -22.0$ (<i>c</i> 1.0, MeOH)	$[\alpha]_D^{25} -23.8$ (<i>c</i> 1.0, MeOH)
¹ H-NMR	500 MHz, D ₂ O	500 MHz, D ₂ O (Appendix B, Figure 20, page 282)
	4.21 (t, <i>J</i> = 7.6 Hz, 1H, H-2)	4.33 (t, <i>J</i> = 7.5 Hz, 1H, H-2)
	3.85 (dd, <i>J</i> = 12.0, 5.7 Hz, 1H, H-9)	3.96 (dd, <i>J</i> = 12.5, 5.5 Hz, 1H, H-9)
	3.78 (dd, <i>J</i> = 12.0, 3.8 Hz, 1H, H-9')	3.91 (dd, <i>J</i> = 12.0, 3.5 Hz, 1H, H-9')
	3.68 (dd, <i>J</i> = 7.6, 6.3 Hz, 1H, H-1)	3.80 (t, <i>J</i> = 7.0 Hz, 1H, H-1)
	3.41 (ddd, <i>J</i> = 7.6, 5.7, 3.8 Hz, 1H, H-3)	3.52 (dd, <i>J</i> = 9.5, 6.5 Hz, 1H, H-3)
	2.73 (m, <i>J</i> = 6.3, 3.2 Hz, 1H, H-5)	2.85-2.82 (m, 1H, H-5)
	2.53-2.60 (m, 1H, H-8a)	2.67-2.64 (m, 1H, H-8a)
	1.84-1.91 (m, 1H, H-8)	2.00 (brd, <i>J</i> = 12.5 Hz, 1H, H-8)
	1.66-1.71 (m, 1H, H-7)	1.81 (brd, <i>J</i> = 13.0 Hz, 1H, H-7)
	1.58-1.63 (m, 1H, H-6')	1.74 (brd, <i>J</i> = 13.0 Hz, 1H, H-6)
	1.26 (qt, <i>J</i> = 13.2, 3.8 Hz, 1H, H-7')	1.42-1.34 (m, 1H, H-7')

Table 4.3. (continued)

	Natural (-)-steviamine (189)	Synthetic [1]
¹ H-NMR	500 MHz, D ₂ O	500 MHz, D ₂ O (Appendix B, Figure 20, page 282)
	1.09-1.12 (m, 1H, H-8')	1.21-1.12 (m ^a , 5H, H-6', H-8' and CH ₃) ^a overlapping of signals
	1.01-1.07 (m, 1H, H-6')	
	1.04 (3H, d, <i>J</i> = 6.3 Hz, CH ₃)	
¹³ C-NMR	126 MHz, D ₂ O	125 MHz, D ₂ O (Appendix B Figure 21, page 282)
	73.8 (C-1)	74.1 (C-1)
	69.1 (C-2)	69.3 (C-2)
	66.7 (C-8a)	66.9 (C-8a)
	61.3 (C-3)	61.5 (C-3)
	56.5 (C-9)	56.7 (C-9)
	52.8 (C-5)	52.8 (C-5)
	33.3 (C-6)	33.6 (C-6)
	29.2 (C-8)	29.5 (C-8)
	23.7 (C-7)	23.9 (C-7)
	19.2 (C-10)	19.4 (C-10)

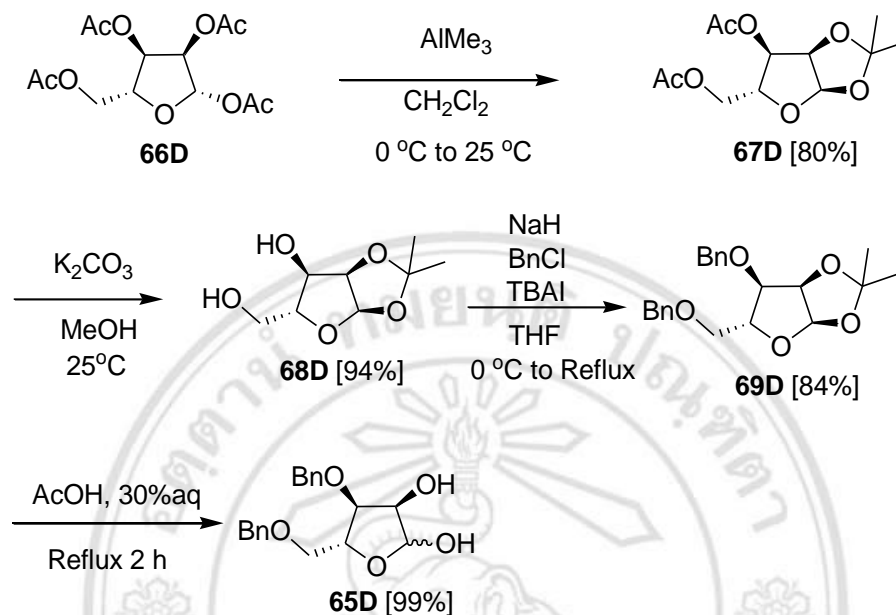
Table 4.3 showed that the NMR spectroscopic data of our synthetic **1**, matched very closely (¹H NMR 0.1 ppm consistent differences, ¹³C NMR 0.04 ppm consistent differences) to those of the natural product. Furthermore, the specific rotation of the synthetic material, $[\alpha]_{\text{D}}^{25} -23.8$ (*c* 1.0, MeOH), was of the same sign and close in magnitude to that of the natural product $[\alpha]_{\text{D}}^{20} -22$ (*c* 1.0, MeOH).

The β -L-ribofuranose 1,2,3,5-tetraacetate derivative [65L] was prepared in four steps and this compound was used as a starting material for the synthesis of 10-*nor*-steviamine [6] and (-)-steviamine [1]. These products were obtained in good overall yields. Therefore, the synthesis of other compounds were planned by changing only one starting material, from the β -L-ribofuranose 1,2,3,5-tetraacetate derivative [65L] to its D-form [65D] and followed the above synthesis protocols to give 10-*nor-ent*-steviamine [83] and 5-*epi-ent*-steviamine [7] (Scheme 4.19).



Scheme 4.19. The synthetic plan for 10-*nor-ent*-steviamine [83] and 5-*epi-ent*-steviamine [7].

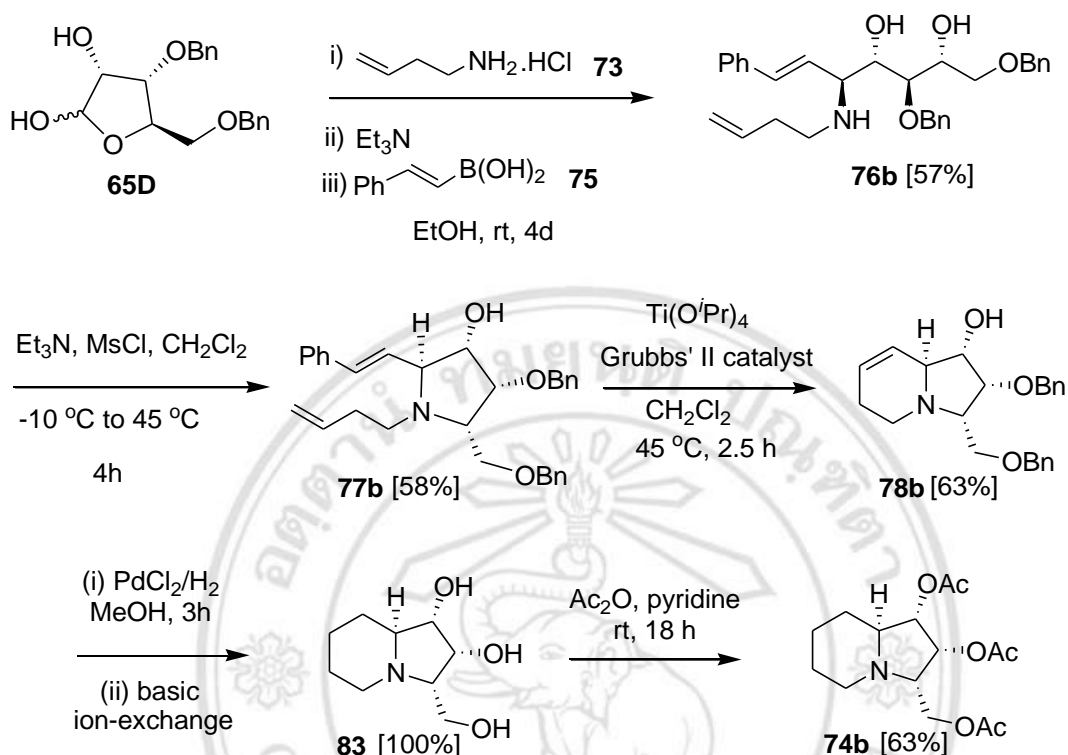
4.4 The synthesis of the β -D-ribofuranose 1,2,3,5-tetraacetate derivative ((3*R*,4*S*,5*R*)-4-(Benzyloxy)-5-(benzyloxymethyl)tetrahydrofuran-2,3-diol) [65D]



Scheme 4.20. The synthesis of the β -D-ribofuranose 1,2,3,5-tetraacetate derivative [65D].

The β -D-ribofuranose 1,2,3,5-tetraacetate derivative [65D] was synthesized in four steps using the same conditions which were used to synthesize the β -L-ribofuranose 1,2,3,5-tetraacetate derivative [65L] (Scheme 4.20). In the first step, treatment a commercially available β -D-ribofuranose 1,2,3,5-tetraacetate [66D] with trimethylaluminium (AlMe_3) in dry CH_2Cl_2 gave, after purification, compound **67D** in 80% yield. In the second step, compound **67D** was deacetylated with K_2CO_3 in MeOH from which the diol [68D] was obtained in 94% yield as a white solid, without further purification. In the third step, the diol [68D] was protected *via O*-benzylation using sodium hydride (NaH), benzyl chloride (BnCl) and tetrabutylammonium iodide (TBAI) in THF . After purification by column chromatography, the expected product [69D] was obtained in 84% yield. In the last step, compound [69D] was hydrolyzed using 30% aqueous acetic acid (AcOH) at reflux for 2 h. The β -D-ribofuranose 1,2,3,5-tetraacetate derivative [65D] was obtained as a white solid (99%) for the synthesis of 10-*nor-ent*-steviamine [83] and 5-*epi-ent*-steviamine [7].

4.5 The synthesis of 10-*nor-ent*-steviamine [83] and its triacetate derivative [74b]



Scheme 4.21. The synthesis of 10-*nor-ent*-steviamine [83] and its acetate derivative [74b].

10-*nor-ent*-steviamine [83], and its triacetate derivative [74b], were prepared in an analogous fashion (Scheme 4.21) to **6** and **74a**, respectively, which started from the Petasis reaction of the β-D-ribofuranose 1,2,3,5-tetraacetate derivative [65D], 3-butenylamine-hydrochloride [73], triethylamine and *trans*-2-phenylvinylboronic acid [75]. The amino diol [76b] was obtained in 57% yield after purification. The ^1H and ^{13}C NMR spectra of **76b** were identical to those of **76a**. They had, as expected optical rotations of the opposite sign. Compound **76b** was cyclized through the *O*-mesylation cyclization using MsCl and triethylamine to afford the fully substituted pyrrolidine [77b] in 58% yield after separation of small amounts of *O,N*-dimesylated **76b** and unreacted **76b** by column chromatography. The pyrrolidine [77b] was reacted with Grubbs' second generation catalyst, in the presence of $\text{Ti}(\text{O}^i\text{-Pr})_4$ via the RCM reaction. The indolizidine [78b] was obtained in 63% yield after purification by column chromatography. In the final step, the hydrogenation/hydrogenolysis of indolizidine

[78b] with PdCl₂/H₂ gave 10-*nor-ent*-steviamine [83] in 100% yield after neutralization and purification by basic ion-exchange chromatography. Moreover, the triacetate derivative [74b] of 10-*nor-ent*-steviamine [83] was also synthesized *via* the acetylation with Ac₂O in dry pyridine. The product was obtained in 63% yield after purification. As we know that 10-*nor-ent*-steviamine [83] and its acetate derivative [74b] are the enantiomers of 10-*nor*-steviamine [6] and its acetate derivative [74a]. The physical properties and the NMR spectral data of 10-*nor-ent*-steviamine [83] and its acetate derivative [74b] were compared with those of 10-*nor*-steviamine [6] and its acetate derivative [74a] as shown in Table 4.4 and Table 4.5.

Table 4.4. Physical and the NMR spectral data of both synthetic 10-*nor*-steviamine [6] and 10-*nor-ent*-steviamine [83].

	10- <i>nor</i> -steviamine [6]	10- <i>nor-ent</i> -steviamine [83]
Structure		
Physical Appearance	yellow oil	brown oil
Optical Rotation	$[\alpha]_D^{25} -7.7$ (<i>c</i> 0.6, H ₂ O) $[\alpha]_D^{25} -11.4$ (<i>c</i> 0.6, MeOH)	$[\alpha]_D^{25} +70.9$ (<i>c</i> 1.0, H ₂ O) $[\alpha]_D^{25} +23.8$ (<i>c</i> 0.6, MeOH)
¹ H-NMR	500 MHz, D ₂ O (Appendix B Figure 7, page 274)	500 MHz, D ₂ O
	4.40 (t, 1H, <i>J</i> = 6.5 Hz, H-2)	4.40 (t, 1H, <i>J</i> 6.5 Hz, H-2)
	3.87 (dd, 1H, <i>J</i> = 12.0, 5.5 Hz, H-9)	3.88 (dd, 1H, <i>J</i> 12.0, 5.5 Hz, H-9)
	3.82 (t, 1H, <i>J</i> = 6.0 Hz, H-1)	3.83 (t, 1H, <i>J</i> 6.5 Hz, H-1)
	3.81 (dd, 1H, <i>J</i> = 12.0, 5.0 Hz, H-9)	3.81 (dd, 1H, <i>J</i> 12.5, 5.0 Hz, H-9)
	3.30 (dd, 1H, <i>J</i> = 12.5, 5.5 Hz, H-3)	3.30 (dd, 1H, <i>J</i> 12.0, 5.0 Hz, H-3)

Table 4.4. (continued)

	10- <i>nor</i> -steviamine [6]	10- <i>nor-ent</i> -steviamine [83]
¹ H-NMR	500 MHz, D ₂ O (Appendix B Figure 7, page 274)	500 MHz, D ₂ O
	2.96-2.93 (m, 1H, H-5)	2.98-2.94 (m, 1H, H-5)
	2.76-2.74 (m, 1H, H-8a)	2.80-2.76 (m, 1H, H-8a)
	2.72-2.67 (m, 1H, H-5)	2.74-2.69 (m, 1H, H-5)
	1.87-1.84 (m, 1H, H-8)	1.88-1.84 (m, 1H, H-8)
	1.80-1.76 (m, 1H, H-7)	1.80-1.76 (m, 1H, H-7)
	1.62-1.58 (m, 1H, H-6)	1.62-1.58 (m, 1H, H-6)
	1.54-1.46 (m, 1H, H-6)	1.55-1.46 (m, 1H, H-6)
	1.41-1.32 (m, 1H, H-7)	1.41-1.32 (m, 1H, H-7)
	1.29-1.21 (m, 1H, H-8)	1.30-1.22 (m, 1H, H-8)
¹³ C-NMR	125 MHz, D ₂ O (Appendix B Figure 8, page 274)	125 MHz, D ₂ O
	74.5 (C-1)	74.7 (C-1)
	70.1 (C-2)	70.4 (C-2)
	64.0 (C-3)	64.4 (C-3)
	63.8 (C-8a)	64.1 (C-8a)
	58.5 (C-9)	58.8 (C-9)
	47.3 (C-5)	47.7 (C-5)
	27.2 (C-8)	27.5 (C-8)
	23.1 (C-6)	23.3 (C-6)
	22.7 (C-7)	22.9 (C-7)

Table 4.5. Physical and the NMR spectral data of both synthetic triacetate derivative of 10-*nor*-steviamine [**74a**] and 10-*nor-ent*-steviamine [**74b**].

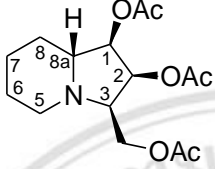
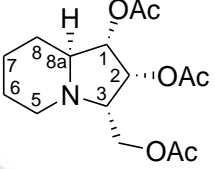
	triacetate derivative of 10- <i>nor</i> -steviamine [74a]	triacetate derivative of 10- <i>nor-ent</i> -steviamine [74b]
Structure		
Physical Appearance	yellow oil	brown oil
Optical Rotation	$[\alpha]_D^{25} +9.4$ (<i>c</i> 0.2, CHCl ₃)	$[\alpha]_D^{25} -9.2$ (<i>c</i> 0.2, CHCl ₃)
¹ H-NMR	500 MHz, CDCl ₃ (Appendix B Figure 11, page 277)	500 MHz, CDCl ₃
	5.44 (t, <i>J</i> = 6.5 Hz, 1H, H-2)	5.45 (t, <i>J</i> = 7.0 Hz, 1H, H-2)
	4.98 (dd, <i>J</i> = 6.5, 4.0 Hz, 1H, H-1)	4.98 (dd, <i>J</i> = 6.5, 4.0 Hz, 1H, H-1)
	4.26 (dd, <i>J</i> = 11.5, 6.5 Hz, 1H, H-9)	4.26 (dd, <i>J</i> = 11.5, 6.0 Hz, 1H, H-9)
	4.09 (dd, <i>J</i> = 11.5, 5.5 Hz, 1H, H-9')	4.09 (dd, <i>J</i> = 11.5, 6.0 Hz, 1H, H-9')
	3.59 (dd, <i>J</i> = 13.0, 6.0 Hz, 1H, H-3)	3.59 (dd, <i>J</i> = 13.0, 6.0 Hz, 1H, H-3)
	3.04 (d, <i>J</i> = 12.5 Hz, 1H, H-5α)	3.04 (d, <i>J</i> = 12.5 Hz, 1H, H-5α)
	2.93 (dt, <i>J</i> = 11.5, 4.0 Hz, 1H, H-8a)	2.94 (dt, <i>J</i> = 11.5, 3.5 Hz, 1H, H-8a)
	2.75-2.69 (m, 1H, H-5β)	2.75-2.70 (m, 1H, H-5β)

Table 4.5. (continued)

	triacetate derivative of 10- <i>nor</i> -steviamine [74a]	triacetate derivative of 10- <i>nor</i> - <i>ent</i> -steviamine [74b]
¹ H-NMR	500 MHz, CDCl ₃ (Appendix B Figure 11, page 277)	500 MHz, CDCl ₃
	2.07 (s, 3H, Ac)	2.08 (s, 3H, Ac)
	2.05 (s, 6H, 2Ac)	2.05 (s, 6H, 2Ac)
	1.82-1.75 (m ^a , 2H, H-6, H8)	1.82-1.75 (m ^a , 2H, H-6, H8)
	1.49-1.42 (m ^a , 2H, H-7)	1.49-1.42 (m ^a , 2H, H-7)
	1.36-1.26 (m, 1H, H-6')	1.36-1.25 (m, 1H, H-6')
	1.23-1.15 (m, 1H, H-8')	1.23-1.15 (m, 1H, H-8')
	^a overlapping of signals	^a overlapping of signals
¹³ C-NMR	125 MHz, CDCl ₃ (Appendix B Figure 12, page 277)	125 MHz, CDCl ₃
	170.8 (C=O)	170.9 (C=O)
	170.4 (C=O)	170.4 (C=O)
	169.9 (C=O)	170.0 (C=O)
	75.3 (C-1)	75.3 (C-1)
	70.2 (C-2)	70.2 (C-2)
	62.8 (C-8a)	62.7 (C-8a)
	61.7 (C-9)	61.7 (C-9)
	59.6 (C-3)	59.5 (C-3)
	47.7 (C-5)	47.7 (C-5)
	28.3 (C-8)	28.2 (C-8)

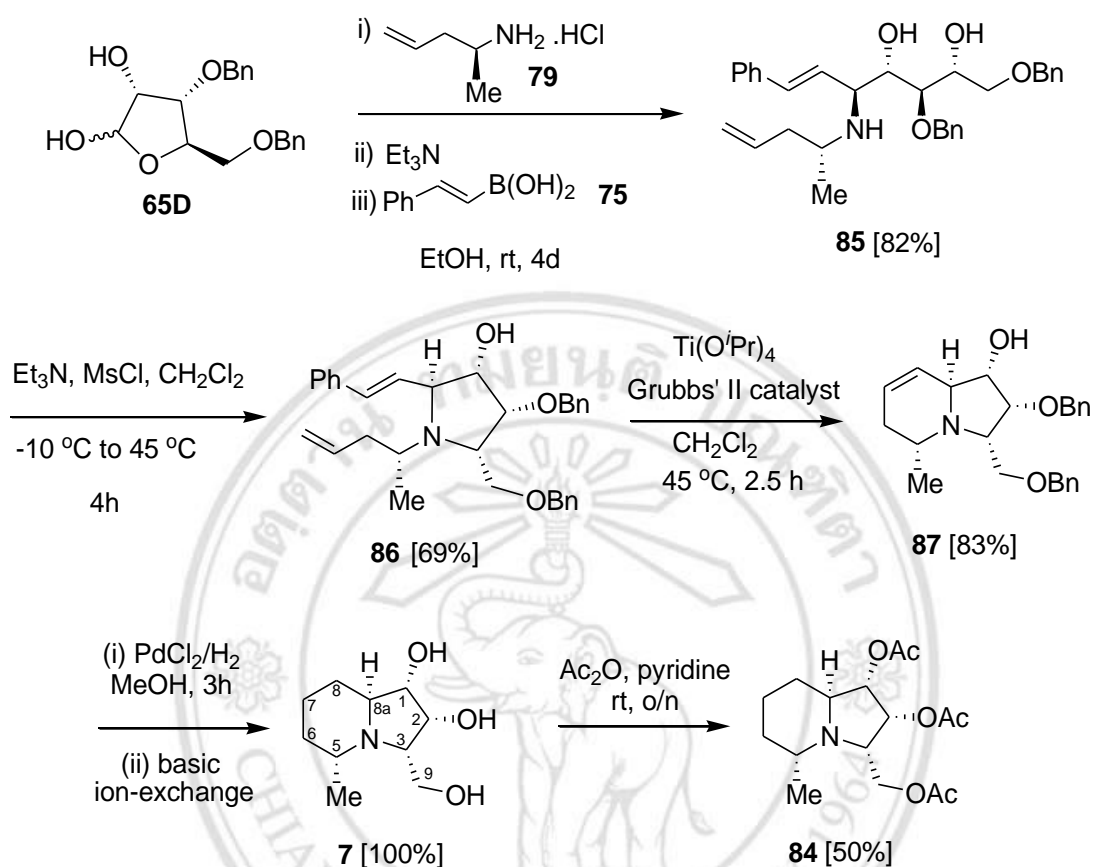
Table 4.5. (continued)

	triacetate derivative of 10- <i>nor</i> -steviamine [74a]	triacetate derivative of 10- <i>nor</i> - <i>ent</i> -steviamine [74b]
¹³ C-NMR	125 MHz, CDCl ₃ (Appendix B Figure 12, page 277)	125 MHz, CDCl ₃
	23.9 (C-6)	23.8 (C-6)
	23.1 (C-7)	23.1 (C-7)
	21.1 (CH ₃)	21.1 (CH ₃)
	20.9 (CH ₃)	21.0 (CH ₃)
	20.7 (CH ₃)	20.7 (CH ₃)

The NMR spectroscopic data of **6** and **83** and those of **74a** and **74b** were identical, allowing for slight spectrometer variations. While the optical rotations of **6** and **83** were opposite in sign they varied significantly in magnitude, however those of compounds **74a** and **74b**, which could be purified on silica gel using organic solvents, were essentially equal and opposite in sign (**74a**: $[\alpha]_{\text{D}}^{25} +9.4$ (*c* 0.2, CHCl₃); **74b**: $[\alpha]_{\text{D}}^{25} -9.2$ (*c* 0.2, CHCl₃)). These results suggested that the samples of **6** and **83** may be different hydrates resulting in incorrect mass measurements when preparing sample for optical rotations. Repeated purifications of these samples did not provide more closely matching specific rotations.

Copyright © by Chiang Mai University
All rights reserved

4.6 The synthesis of 5-*epi-ent*-steviamine [7] and its triacetate derivative [84]



Scheme 4.22. The synthesis of 5-*epi-ent*-steviamine [7] and its triacetate derivative [84].

For the synthesis of 5-*epi-ent*-steviamine [7] (Scheme 4.22), the β-D-ribofuranose 1,2,3,5-tetraacetate derivative [65D] was treated with (*R*)-4-penten-2-amine·HCl [79], triethylamine and *trans*-2-phenylvinylboronic acid [75] in EtOH at rt for 4 days to give the amino diol [85] in 82% yield after purification. The *O*-mesylation cyclization of the amino diol [85] using MsCl and triethylamine afforded the fully substituted pyrrolidine [86] in 69% yield after separation of small amounts of *O,N*-dimesylated 85 and the unreacted 85 by column chromatography. The RCM of the pyrrolidine [86] used Grubbs' second generation catalyst, in the presence of Ti(*Oⁱ*-Pr)₄ to afford the indolizidine [87] in 83% yield after purification by column chromatography. In the last step, the hydrogenation/hydrogenolysis of indolizidine [87] with PdCl₂/H₂ gave 5-*epi-ent*-steviamine [7] in 100% yield after neutralization and purification by basic ion-

exchange chromatography. In addition, its triacetate derivative [84] was also prepared with Ac₂O in dry pyridine *via* the acetylation reaction. The desired product was obtained in 50% yield after purification. *5-Epi-ent-steviamine* [7] has been synthesized by Hu *et al.* in 2010 (193). Therefore, the physical properties and the NMR spectral data between this literature and the synthetic *5-epi-ent-steviamine* [7] were compared and summarized in Table 4.6.

Table 4.6. Physical and the NMR spectral data of the literature (193) and *5-epi-ent-steviamine* [7].

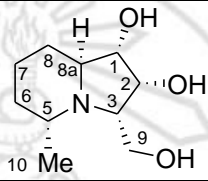
	<i>5-epi-(+)-steviamine</i> (193)	Synthetic <i>5-epi-ent-steviamine</i> [7]
Structure		
Physical Appearance	Yellow oil	Brown oil
Optical Rotation	$[\alpha]_D^{20} -1.2$ (<i>c</i> 1.0, MeOH)	$[\alpha]_D^{25} -4.6$ (<i>c</i> 1.0, MeOH)
¹ H-NMR	300 MHz, D ₂ O	500 MHz, D ₂ O (Appendix B, Figure 28, page 286)
	4.32 (t, <i>J</i> = 5.7 Hz, 1H)	4.37 (t, <i>J</i> = 6.0 Hz, 1H, H-2)
	4.05 (dd, <i>J</i> = 10.2, 5.1 Hz, 1H)	4.09 (dd, <i>J</i> = 10.5, 5.5 Hz, 1H, H-1)
	3.72 (dd, <i>J</i> = 11.1, 8.4 Hz, 1H)	3.77 (dd, <i>J</i> = 11.0, 9.5 Hz, 1H, H-9)
	3.56 (dd, <i>J</i> = 11.1, 5.7 Hz, 1H)	3.60 (dd, <i>J</i> = 11.0, 5.5 Hz, 1H, H-9')
	3.33 (dt, <i>J</i> = 8.4, 5.7 Hz, 1H)	3.29-3.25 (m, 1H, H-3)
	3.04-3.00 (m, 1H)	3.00-2.97 (m, 1H, H-8a)
	2.59-2.57 (m, 1H)	2.55-2.51 (m, 1H, H-5)
	1.68-1.58 (m, 3H)	1.77-1.75 (m, 1H, H-8)
	1.50-1.09 (m, 2H)	1.71-1.63 (m ^a , 2H, H-6, H-8')

Table 4.6. (continued)

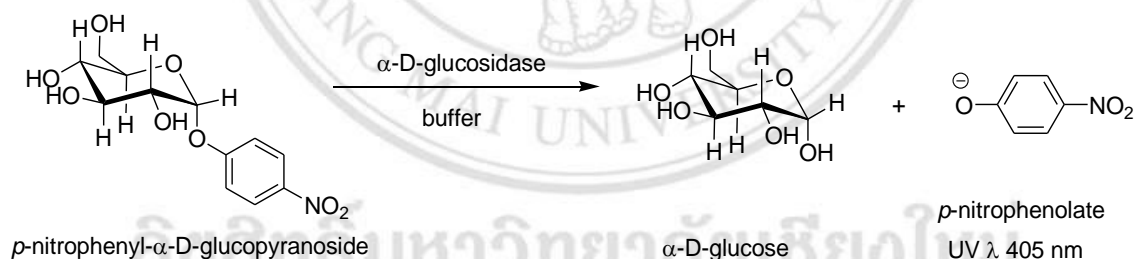
	<i>5-epi-(+)-steviamine</i> (193)	Synthetic <i>5-epi-ent-steviamine</i> [7]
¹ H-NMR	300 MHz, D ₂ O	500 MHz, D ₂ O (Appendix B, Figure 28, page 286)
	1.00 (d, <i>J</i> = 5.7 Hz, 3H)	1.56-1.52 (m, 1H, H-7)
		1.45-1.37 (m, 1H, H-7')
		1.16-1.08 (m, 1H, H-6')
		1.02 (d, <i>J</i> = 6.0 Hz, 3H, CH ₃)
		^a overlapping of signals
¹³ C-NMR	75 MHz, D ₂ O	125 MHz, D ₂ O (Appendix B Figure 29, page 286)
	70.4	70.6 (C-1)
	69.6	69.8 (C-2)
	66.6	66.2 (C-3)
	60.1	60.4 (C-9)
	58.8	58.5 (C-8a)
	55.5	55.1 (C-5)
	31.6	32.0 (C-6)
	22.5	22.7 (C-8)
	19.9	20.4 (CH ₃)
	17.7	18.1 (C-7)

The NMR spectroscopic data of **7** agreed well with those in the literature (193). The specific rotation of **7** ($[\alpha]_{\text{D}}^{25} -4.6$ (*c* 1.0, MeOH)) was of the same sign and of similar low magnitude to that reported ($[\alpha]_{\text{D}}^{20} -1.2$ (*c* 1.0, MeOH)). We therefore can conclude that their structure were identical.

4.7 Glycosidase inhibitory assay

Synthetic (–)-steviamine [1], 10-*nor*-steviamine [6], 10-*nor-ent*-steviamine [83] and 5-*epi-ent*-steviamine [7] were tested for their glycosidase inhibitory activities using commercially available enzymes and *p*-nitrophenyl substrates. All enzymes were assayed at 27 °C in 0.1 M citric acid / 0.2 M disodium hydrogen phosphate buffers at the optimum pH for each enzyme. The incubation mixture was 10 μL enzyme solution, 10 μL of 1 mg/mL aqueous solution of the test compound and 50 μL of *p*-nitrophenyl substrate (5 mM). The reactions were stopped by addition of 70 μL 0.4 M glycine (pH 10.4) and their absorbances were recorded at 405 nm using a Versamax microplate reader (Molecular Devices) (258).

The quantity of *p*-nitrophenolate produced in each assay was measured by UV-vis spectrophotometry in order to determine the effect of varying concentration of the inhibitor (test compound). Theoretically, one molecule of *p*-nitrophenol is liberated for each enzymatic cleavage of the sugar substrate. Upon treatment with glycine buffer (pH 10.4), *p*-nitrophenol is converted to its corresponding *p*-nitrophenolate anion, which has a known extinction coefficient at 405 nm (Scheme 4.23)



Scheme 4.23. Mechanism of the glycosidase inhibitory activity assay.

The results of the glycosidase inhibitor testing for (–)-steviamine **1**, its analogues: 10-*nor*-steviamine [6], 10-*nor-ent*-steviamine [83] and 5-*epi-ent*-steviamine [7] and swainsonine [2], *ent*-**2** and castanospermine [3] against twelve glycosidases are shown in Table 4.7. These mean % inhibition tests were determined for each compound at 143 μg/mL according to the previously published protocols (258).

Table 4.7 The glycosidase inhibition of compounds **1**, **6**, **7** and **83** (Mean % Inhibition at 143 µg/mL).

Enzyme (Source, pH)	1	6	7	83	2	ent-2	3
α -D-glucosidase (<i>Saccharomyces cerevisiae</i> , 6.8)	0	0	0	5	0	3	0
α -D-glucosidase (<i>Bacillus sterothermophilus</i> , 6.8)	-27	22	18	-38	0	15	80
α -D-glucosidase (rice, 4.0)	-6	-8	-9	-6	12	2	6
β -D-glucosidase (Almond (<i>Prunus</i> sp.), 5.0)	0	11	0	0	0	2	90
α -D-galactosidase (Green coffee bean (<i>Coffea</i> sp.), 6.5)	0	12	-15	0	-4	1	-3
β -D-galactosidase (Bovine liver, 7.3)	0	19	6	20	-3	7	16
α -D-mannosidase (Jack bean (<i>Canavalia ensiformis</i>), 4.5)	11	31	0	9	11	100	9
β -D-mannosidase (<i>Cellulomonas fimi</i> , 6.5)	-13	0	0	0	2	-5	-
α -L-rhamnosidase (<i>Penicillium decumbens</i> , 4.0)	6	53	20	50	100	4	39
<i>N</i> -acetyl- β -D-glucosaminidase (Bovine kidney, 4.25)	0	-9	0	-19	13	5	-
<i>N</i> -acetyl- β -D-glucosaminidase (Jack bean, 5.0)	11	51	30	-17	3	24	-
β -glucuronidase (Bovine liver, 5.0)	-5	0	0	0	-	-	-

In general compounds **1**, **6-7** and **83** were found to have poor to moderate inhibitory activity against most enzymes. None were as active as (-)-swainsonine [**2**] against α -L-rhamnosidase (from *Penicillium decumbens*) or (+)-swainsonine (*ent-2*) against α -D-mannosidase (from Jack bean) or castanospermine [**3**] against α -D-glycosidase (from *Bacillus sterothermophilus*) and β -D-glycosidase (from Almond). The 10-*nor* analogues, **6** and **83**, however, showed 50 and 53% inhibition of α -L-rhamnosidase from *Penicillium decumbens* while 10-*nor*-steviamine [**6**], showed 51% inhibition of *N*-acetyl- β -D-glucosaminidase (from Jack bean) at the same concentration (760 μ M). It is interesting that the enantiomeric compounds **6** and **83** gave almost equal inhibition of α -L-rhamnosidase whereas **1** and **7**, with the extra methyl group, is a much weaker inhibitor. Both **6** and **83** have two equivalent hydroxyls to *ent*-swainsonine (*ent-2*) and swainsonine [**2**], respectively and yet they both follow *ent*-swainsonine in inhibition of α -L-rhamnosidase and not α -D-mannosidase. The natural (-)-steviamine (193) showed weak inhibition of β -glucosidases from almond and *Caldocellum saccharolyticum* with IC₅₀ values of 454 and 739 μ M, respectively and it also exhibited weak inhibition of an *R*-galactosaminidase (GalNAcase) with IC₅₀ value of 814 μ M. The synthetic (-)-steviamine [**1**] does not show significant inhibition of any glycosidase tested; it may have a biological function in the source plant inhibiting a glycosidase we have not tested against or it is clear that iminosugars can be functional without glycosidase inhibition and in fact this lack of glycosidase inhibition (or high selectivity) may make them more suitable as pharmaceutical products (266).

Interestingly, all compounds appeared to promote the activities of certain enzymes. In particular, compounds **1** and **83** seemed to significantly promote the activity of α -D-glucosidase (from *Bacillus sterothermophilus*). This promotion of activity could be due to enzyme stabilization or improved folding of the enzyme via non-catalytic site binding.

The inhibitory activity of compound **6**, which was prepared previously (194), and had different NMR properties to this synthetic, was reported to have no inhibitory activity against two α -D-glucosidases (from Baker's yeast and rice), one β -D-glucosidase (from sweet almonds) and a β -D-galactosidase (from bovine liver). These results are

consistent with the results shown in Table 4.7. The earlier report showed that compound **6** was a more significant inhibitor of α -L-rhamnosidase (from *Penicillium decumbens*, IC₅₀ 35 μ M)) and α -D-mannosidase (from Jack bean, IC₅₀ 82 μ M)) and a significantly weaker inhibitor of α -L-fucosidase (from bovine kidney, IC₅₀ 593 μ M)). In this study, the synthetic compound **6** also showed some, although very weak, activity against α -D-mannosidase (from Jack bean, only 31% inhibition at 760 μ M, Table 4.7) and an IC₅₀ of approximately 760 μ M (53% inhibition) against the α -L-rhamnosidase from *Penicillium decumbens*.

The glycosidase inhibitory activity of compound **7**, which was synthesized by Hu *et al.* (193), was reported to be a significant inhibitor of α -L-rhamnosidase (from *Penicillium decumbens*, IC₅₀ 342 μ M)) and have no inhibitory activity against β -D-glucosidase (from almond) and *N*-acetyl- β -D-glucosaminidase (from Jack bean). In this study, the synthetic compound **7** showed similar results which inhibited α -L-rhamnosidase (from *Penicillium decumbens*, 20% inhibition at 708 μ M, Table 4.7) and has no inhibition against β -D-glucosidase (from almond), but it showed 30% inhibition against *N*-acetyl- β -D-glucosaminidase (from Jack bean). Moreover, this synthetic compound **7** (708 μ M) has no inhibition against α -D-mannosidase (from Jack bean) and seemed to slightly promote α -D-glucosidase (from rice) and α -D-galactosidase (from Green coffee bean), while the previous synthetic compound **7** showed significantly weak inhibition of all these enzymes (at 1000 μ M) (193).

ลิขสิทธิ์มหาวิทยาลัยเชียงใหม่
Copyright© by Chiang Mai University
All rights reserved